Experimental Study of Tsunami-Like Waves Generated with a Vertical Release Technique on Dry and Wet Beds

Davide Wüthrich[1]; Michael Pfister[2]; Ioan Nistor, M.ASCE[3]; and Anton J. Schleiss, M.ASCE[4]

Abstract: Tsunamis, impulse waves, and dam failures are disasters that challenge humanity, often leading to massive casualties and extreme economic losses. The highly unsteady flow conditions generated by such events are often in the form of turbulent bores. The purpose of this study was to investigate and validate a new generation system for bores propagating over dry and wet bed conditions. There are multiple techniques to generate such waves experimentally, and the study focused on the generation of tsunami-like inundation conditions through the vertical release of a water volume. A detailed methodology to characterize the generated waves hydraulically, in terms of their wave heights and flow velocities, is presented, and good agreement with the classical dam-break case for both dry bed surges and wet bed bores was demonstrated. Because of the importance of estimating the impact forces induced by such waves, particular attention was given to the wavefront celerity and the velocity profiles measured behind the wavefront; these were found in agreement with Prandtl's power law for open channel flows, and in-depth measurements allowed for the definition of an expression to estimate flow deceleration behind the wavefront. Along with considerations of the Froude number and momentum, this paper provides relevant information to assist engineers in designing safer infrastructures in areas prone to such extreme loading. **DOI: 10.1061/(ASCE)WW.1943-5460.0000447.** © *2018 American Society of Civil Engineers.*

Author keywords: Dam break; Tsunami; Dry bed surge; Wet bed bore; Velocity profiles; Momentum.

Introduction

Relevance

Tsunamis, impulse waves, and dam-break waves are rare phenomena. Therefore, visual observations of prototype events are rare and often difficult to assess during their occurrence. Nevertheless, some recent episodes, such as the 2004 Indian Ocean tsunami and the 2011 Tōhoku tsunami in Japan, allowed for the comparison of theoretical solutions with posttsunami data collected through postevent field surveys and forensic engineering surveys (Chanson 2006; Chock et al. 2013). Most of the recent studies focused on the tsunami inundation depths and velocities (Dias et al. 2006; Matsutomi et al. 2006; Rossetto et al. 2007; Fritz et al. 2012; Jaffe et al. 2012) and showed a wide range of magnitudes, with maximum velocities up to 13 m/s near the Sendai Airport (Jaffe et al. 2012) and inundation depths of more than 15 m in the City of Onagawa (Suppasri et al. 2013).

In mountain areas, landslide-induced waves are characterized by short wavelengths and great impulsiveness. Such was the case of the Vajont Dam (Italy) event, where a landslide into the reservoir generated a sudden overflow of the dam crest by a wave as high as 245 m (Kilburna and Petleyb 2003). The released discharge fell into the narrow downstream valley, resulting in a massive wave that caused the death of more than 2,000 people, leaving the dam almost undamaged, as shown in Fig. 1.

In addition, storm surges, tidal bores, or collapse of artificial and natural dams or dikes can generate flows with similarly drastic consequences. The diversity and heterogeneity are reflected in the several generation techniques used to reproduce these flows in a laboratory environment, including wave pistons, landslide generators, pump-driven generators, vertical releases, and dam-break gates (vertical lift or swing type).

In this study, a controlled vertical release technique was used such that a water volume dropped from an upper reservoir into a lower one resulted in the formation of a turbulent bore. Similar techniques were previously used by Chanson et al. (2002, 2003), Meile (2007), and Meile et al. (2008, 2011). The main advantage of the vertical release technique used in the present study was its flexibility in controlling both the volume and the released discharge, allowing for reproduction of surges and bores with different flow depths and propagation velocities.

Independently of the generating mechanism, the main hydrodynamic properties of the propagating bore and surge were affected by the dry or wet bed conditions of the channel. The difference in behavior between dry and wet surfaces was shown experimentally by Lauber and Hager (1998), Ramsden (1993), and Nouri et al. (2010), among others. A wave propagating on a dry bed is commonly called a *surge*; whereas, because of its turbulent and an aerated appearance, a wave on a wet bed is termed a *bore*. An example

[1]Doctoral Student, Laboratory of Hydraulic Constructions (LCH), School of Architecture, Civil and Environment Engineering (ENAC), Ecole Polytechnique Fédérale de Lausanne (EPFL), Station 18, 1015 Lausanne, Switzerland (corresponding author). E-mail: davide.wuthrich@epfl.ch

[2]Professor, Civil Engineering Dept., Haute Ecole d'Ingénierie et d'Architecture de Fribourg (HEIA-FR, HES-SO), 1700 Fribourg, Switzerland. E-mail: michael.pfister@hefr.ch

[3]Professor, Dept. of Civil Engineering, Univ. of Ottawa, 161 Louis-Pasteur, A110, Ottawa, ON, Canada K1N 6N5. E-mail: inistor@uottawa.ca

[4]Professor, Laboratory of Hydraulic Constructions (LCH), School of Architecture, Civil and Environment Engineering (ENAC), Ecole Polytechnique Fédérale de Lausanne (EPFL), Station 18, 1015 Lausanne, Switzerland. E-mail: anton.schleiss@epfl.ch

Note. This manuscript was submitted on March 21, 2017; approved on December 11, 2017; published online on April 23, 2018. Discussion period open until September 23, 2018; separate discussions must be submitted for individual papers. This paper is part of the ***Journal of Waterway, Port, Coastal, and Ocean Engineering***, © ASCE, ISSN 0733-950X.

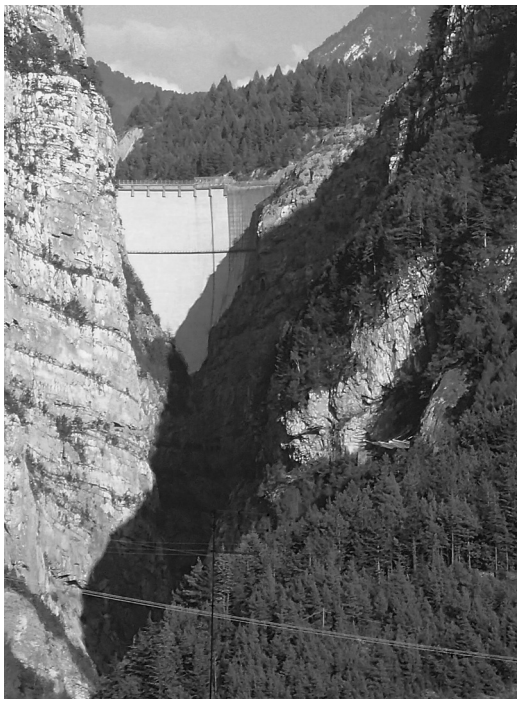

Fig. 1. Vajont Dam located in northwest Italy, 53 years after the impulse wave which occurred in October 1963. (Image by Davide Wüthrich, September 2016.)

in nature of this difference can be observed in Fig. 2, which shows the case of a tidal bore propagating upstream in the Garonne River in France on both dry and wet bed conditions.

Long-Wave Generation Techniques

Various techniques can be used to reproduce surges and bores in models. A comprehensive literature review of these techniques was presented by Liu et al. (2008). Previous experimental studies used mostly solitary waves to reproduce tsunami and impulse waves; these were obtained through piston-type wave generators. The use of solitary waves was criticized by Madsen et al. (2008) because of the short wavelength and period compared with real tsunami waves. The transition between solitary waves and overland flow was addressed by Fuchs and Hager (2015).

Currently, the use of dam-break waves generated through the sudden release of water impounded behind a vertical wall is considered a more appropriate method to reproduce the inundation generated by tsunamis and impulse waves (Chanson 2005, 2006). The dam-break technique was used by several authors, including Cross (1967), Yeh et al. (1989), Arnason et al. (2009), Nistor et al. (2009), and O'Donoghue et al. (2010), among others. The sudden opening can be achieved through vertical lift gates (Lauber and Hager 1998) or swing gates (Goseberg et al. 2017). This approach was based on the theory of Ritter (1892), and it assumed a semifinite reservoir, ideal fluid conditions, and a wave propagating on a smooth horizontal channel. At the tip of the wave, friction became nonnegligible (Chanson 2005), and a modified dam-break theory was developed by Whitham (1955) and Chanson (2009).

Landslide-generated waves were often reproduced through the sudden drop of a solid, granular, or liquid body into the water, producing a wave traveling away from the generation location. This technique was particularly suitable to reproduce impulse

Fig. 2. Tidal bore at Podensac (France) on the Garonne River. The picture shows an example of the difference in behavior for a bore propagating over dry bed (left side, over the bank) and over wet bed (right side, near the surfer). (Image by Davide Wüthrich, October 2015.)

waves. A landslide generator can function either manually, by dropping a solid block inside the water (Thusyanthan and Madabhushi 2008), or with a more sophisticated mechanism, such as a pneumatic landslide generator (Fritz 2002). The drop of a granular body inside the reservoir was previously used by Huber (1980), Fritz (2002), and Heller (2007), among others. Goseberg et al. (2013) introduced the concept of a pump-driven long-wave generation technique as an alternative approach to generate long-period waves in the laboratory. Furthermore, positive surges and bores in rivers and artificial channels can be reproduced through the sudden closure of a downstream gate (Koch and Chanson 2009; Leng and Chanson 2017b).

A vertical release through the sudden drop of a volume of water was also used to generate tsunami-like waves (Chanson et al. 2002, 2003; Meile 2007; Rossetto et al. 2011). At present, some of the newest large-scale facilities apply a similar concept to reproduce controlled long-period waves using pneumatic tsunami simulators (Allsop et al. 2014; Chandler et al. 2016).

Objective, Novelty of the Study, and Outline

The main objectives of this research were as follows:

- To present and discuss the hydraulic behavior of dry bed surges and wet bed bores generated using the vertical release technique;
- To compare the generated surges and bores with existing theories developed for classical dam-break waves;
- To provide insights on the hydrodynamic behaviors of surges and bores in terms of front celerity, velocity profiles, and deceleration behind the wavefront; and
- To present and discuss the temporal behavior of the Froude number and the momentum flux per unit width for both surges and bores.

The outline of the paper is as follows: After an explanation of the wave-generation technique and instrumentation used, tests performed and the methodology followed throughout the study are described. The next section focuses on the longitudinal profiles of the produced waves before the explanations of the velocities, Froude number, and momentum flux. The "Discussion" and "Conclusions" sections describe the key findings of this study.

Experimental Setup and Acquisition System

Tests were performed at the Laboratory of Hydraulic Constructions (LCH) at Ecole Polytechnique Fédérale de Lausanne (EPFL) in Switzerland. A vertical release technique was used to generate surges propagating over a dry bed and bores propagating over a wet bed. This experimental facility implemented the setup previously used by Meile (2007) and Meile et al. (2008, 2011). Compared to the previous studies cited, the released discharge was higher for this study, and a new downstream channel was built; nevertheless, the upstream and downstream reservoirs were the same as those in the previous work.

Vertical Release Generation Technique

A $2.1 \times 3.0 \times 1.0$-m upper reservoir with a total storage volume of 7.08 m^3 was connected to a water-filled lower reservoir through three newly installed, identical, and independent PVC pipes, each with an internal diameter of 315 mm (Fig. 3). The pipes were symmetrical to the central axis of the channel with a transversal distance of 0.45 m between adjacent pipes [Fig. 3(a)]. Each pipe was independently fitted with a valve, and the sudden water release was achieved through a system of pulleys and Vectran-fiber ropes with a diameter of 0.01 m and a maximum elastic extension of less than 1%. All ropes were connected to the same handle, thus ensuring a synchronized opening of all valves [Fig. 3(b)]. The release mechanism is shown in Fig. 3(b). The total difference in the head between the upstream and the downstream reservoir, ΔH, was 2.1 m.

When the generation system was activated (i.e., the ropes were released and valves opened), a difference in the head between the upper and lower reservoir was established [Fig. 4(b)], resulting into a gravitational flow through the pipes. Since the lower basin was completely filled with water, the incoming discharge resulted in an upward flow at the channel inlet, and subsequently, a free-surface wave formed and propagated downstream in the flume. A schematic of the release mechanism and the resulting flow in the lower reservoir is presented in Fig. 4. All waves propagated over a smooth horizontal channel with a length of 15.5 m and a width of 1.4 m. On average, the Darcy-Weisbach friction factor of the channel, f, was measured to be 0.021 using steady-state experiments under various flow conditions. This factor corresponded to an average roughness, k_s of 0.66 mm, which was consistent with the values suggested by

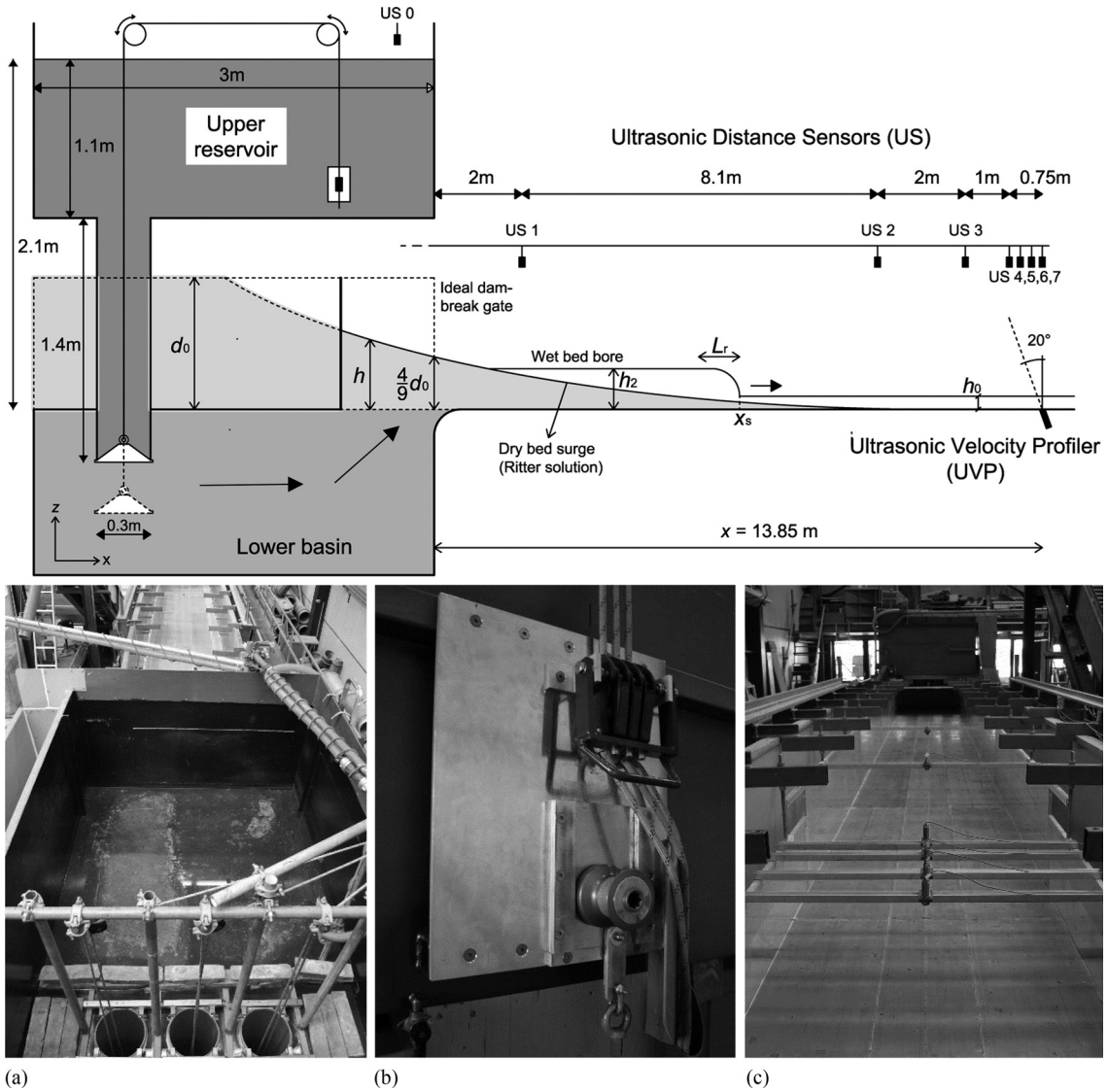

Fig. 3. Experimental set-up and instrumentation used in the present study: (a) upper reservoir with pipes; (b) release mechanism and handle; (c) channel (upstream view) (Images by Davide Wüthrich.)

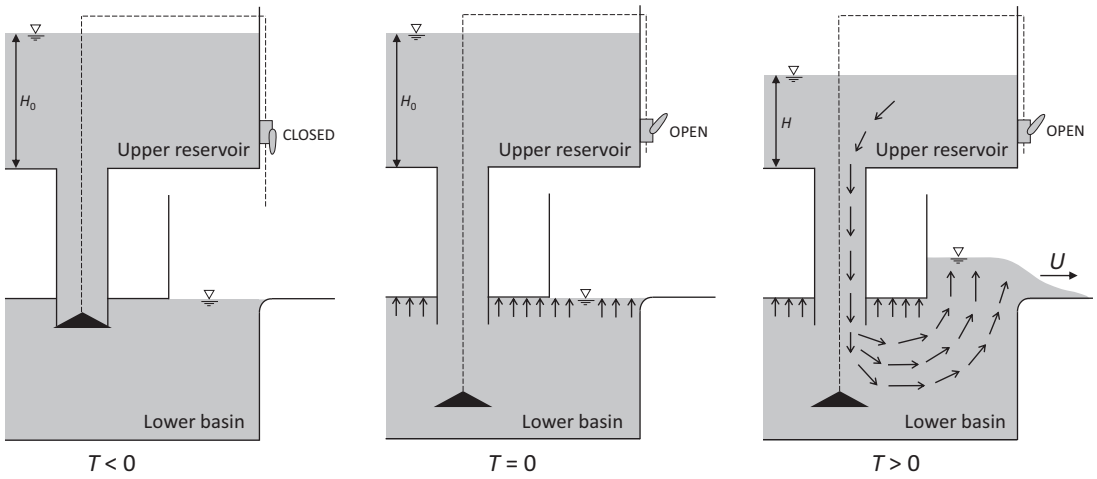

Fig. 4. Release mechanism and flow behavior before ($T < 0$), during ($T = 0$), and after ($T > 0$) the opening of the gates

Henderson (1966). The water was evacuated at the downstream end of the flume, thus avoiding any backwater effect. For the generation of wet bed bores, an initial still water depth, h_0, on the flume (*wet bed* condition) was ensured using a vertical sill located at the downstream end of the channel.

Instrumentation and Acquisition System

The flow depth of the propagating waves was measured using seven ultrasonic distance sensors (USs), type UNAM 30I6103 from Baumer (Frauenfeld, Switzerland), with a measuring range between 100 and 1,000 mm. The USs were located along the channel at x of 2, 10.10, 12.10, 13.10, 13.35, 13.60, and 13.85 m from the flume inlet (Fig. 3), which was the origin of the system of coordinates, and sampled at an acquisition frequency of 12.5 Hz with an accuracy of 0.5 mm and a response time of less than 80 ms. The arrangement of sensors from US4 to US7 was chosen to ensure a higher measurement density between x of 13.1 and 13.85 m, thus providing a more precise description of the shape of the propagating wave. The minimal required distance between two adjacent sensors to avoid interference was conservatively respected. An additional sensor (US0) from the Baumer UNAM 50 series with an extended measuring range (250–4,000 mm) was installed in the upper reservoir to ensure the accurate recording of the opening time of the system ($t = 0$ s). For all tests, the opening time was selected when a decrease of 0.01 m was observed in the upper reservoir. A shifted time based on the surge or bore arrival time was defined as $T = t - t_0$.

Flow velocities were investigated using an ultrasound velocity profiler (UVP-DUO) produced by Met-Flow (Lausanne, Switzerland); this instrument provided instantaneous flow velocity profiles along the transducer axis by detecting the Doppler shift frequency of echoed ultrasound as a function of time. The chosen transducer had an emitting frequency of 2 MHz, was installed within the channel bottom pointing in the upstream direction with an inclination of 20° with respect to the vertical, and was located at a horizontal distance, x, of 13.85 m from the channel inlet (Fig. 3). One UVP per cross section was used, and measurements were taken in the transducer axis direction, then projected in the main flow direction (x-axis). Velocity components in the vertical and transversal directions were not considered. A sensitivity analysis of the main parameters involved in the UVP acquisition system was performed by Wüthrich et al. (2016a). As a result, the number of repetitions per profile (within the same measure) was selected as 128, leading to acquisition frequencies ranging between 12.5 and 55 Hz, corresponding to measurement durations of 80–18 ms and to an accuracy of approximately 10 mm/s throughout the entire water column. The acoustic scattering was enhanced by means of a hydrogen-bubble-generation technique similarly to Blanckaert and Lemmin (2006) and Meile et al. (2008). The hydrogen bubbles were produced through electrolysis at a distance of 1.5 m from the channel inlet, to ensure sufficient mixing for a uniform distribution in the vertical direction. High speed photos and videos were used to record the time and spatial development of the waves.

All data were acquired by means of the *LabVIEW* data-acquisition system. All USs were directly connected to the *LabVIEW* master program, and the synchronization with the UVP-DUO unit was achieved through a transistor-transistor logic (TTL)–level (+5 V, minimum 20 ns) trigger signal, sent when the measure was launched from the main panel. This synchronization time was estimated to be less than 3 ms, which is short compared to the measurement duration of both instruments. This method allowed for the same time reference to be initially set for both instruments, ensuring that every velocity profile was associated to the corresponding flow depth.

Analogy with Dam-Break Waves

Preliminary tests showed the key role of the initial discharge, Q_0, released into the channel for the definition of the main hydrodynamic properties of the produced wave. The use of 1, 2, or 3 pipes, denoted as n, for the sudden release of water allowed for the control of the initial discharge Q_0, producing surges and bores with different values of wave height, h, and front celerity, U. A comparison with the theoretical solution proposed by Ritter (1892) for dam-break waves was conducted. Similar to what was discussed by Chanson et al. (2002), through the initial discharge Q_0, an equivalent impoundment depth, d_0, was obtained as

$$d_0 = \frac{9}{4}\left(\frac{Q_0^2}{gB^2}\right)^{1/3} \tag{1}$$

where g = gravity constant; B = channel width; and Q_0 = initial discharge released into the channel. From Eq. (1), d_0 was calculated as the outflow discharge from the upper reservoir, obtained as a function of dH/dt, where H is the water depth measured by US0 (Fig. 4). The graphs obtained for all three scenarios (one, two, and three pipes) are shown in Fig. 5(a) and the computed values of Q_0 are

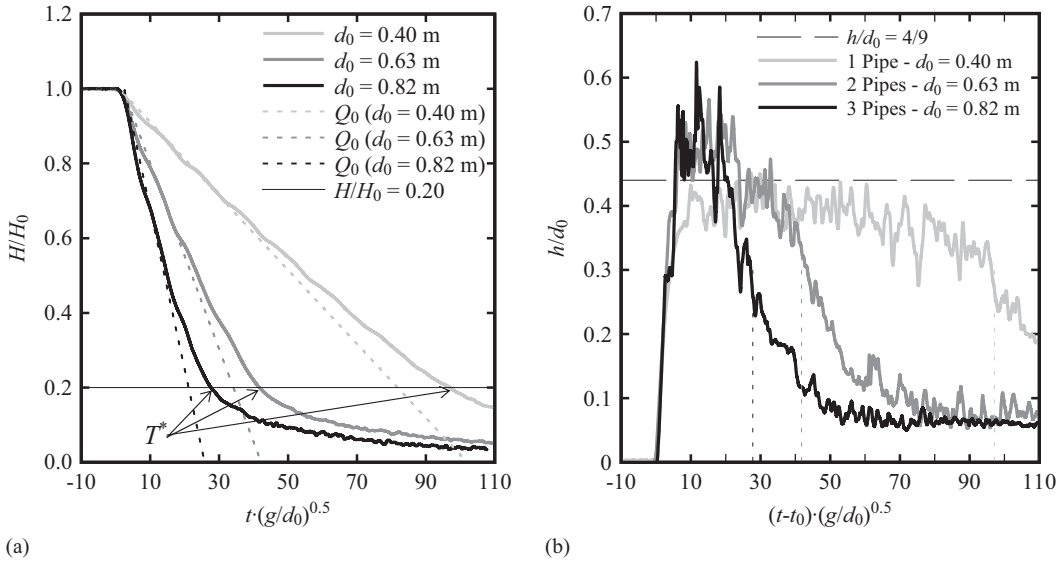

Fig. 5. Measurements of the water depth for three dry bed surges generated with the vertical release technique using one, two, and three pipes in Tests 3, 2, and 1, respectively: (a) upstream reservoir; (b) channel inlet (x = 0 m) (Note: the values of the released discharges are presented in Table 1)

Table 1. Equivalent Impoundment Depths Obtained for the Vertical Release Technique through the Progressive Use of One, Two, and Three Pipes

Number of pipes	Pipe surface [A_P (m^2)]	Head (m)	Initial discharge [Q_0 (m^3/s)]	Equivalent impoundment depth [d_0 (m)]	T^*
1	0.073	2.10	0.34	0.40	97.1
2	0.146	2.10	0.68	0.63	41.8
3	0.219	2.10	1.03	0.82	27.8

presented in Table 1. Given the nonlinear behavior of the reservoir-emptying process, the chosen values showed good agreement during the initial time, leading to some error in the later phases of the test. Thus, T^* was defined as the dimensionless time after which the hypothesis of a continuously released discharge was no longer acceptable (H/H_0 = 0.2). These initial discharges were also successfully compared with the theoretical values using the continuity equation $Q_0 = A_P \cdot V_P$, where A_P is the pipe surface and V_P is the velocity through the pipes, $V_P = \sqrt{2g(\Delta H - \xi \Delta H)}$. The head loss at the inlet of the pipes, ξ, was assumed to be 0.5. If the friction losses through the PVC pipes and those in the trajectory between the pipes and the channel inlet are neglected, then the initial discharge is $Q_0 = A_P \cdot \sqrt{2g\Delta H}$ (Table 1).

For a constant volume in the upper reservoir, a smaller released discharge allowed for a longer time before the sudden reduction took place, resulting in waves with a longer duration. Higher discharges were associated with shorter durations, and the generated waves were characterized by an impulse behavior.

Measurements of the water depth at the channel inlet (x = 0 m) were made to validate the comparison to the theory of Ritter (1892). The use of an additional US at x = 0 m allowed for the capture of the oscillating behavior of the flow around a h/d_0 value of 4/9, as shown in Fig. 5, for the scenarios with one, two, and three pipes. These findings are similar to what was predicted by Ritter (1892) for an infinite reservoir, implying close similarity between surges and bores produced with the classical dam-break and with the vertical release techniques. Fig. 5(b) shows that, after a certain time, the measured flow depth in the channel suddenly decreased as a consequence of the emptying of the upstream reservoir [Fig. 5(a)].

Experimental Methodology

The purpose of this study was to characterize the generation and propagation of experimentally generated bores and surges in terms of depth and velocity. The main experimental parameters varied were the initial discharge Q_0 (the equivalent impoundment depth d_0) and the initial still water depth h_0. Thirty-eight tests were conducted in this study, as listed in Table 2. For the wet bed bores, all tests were performed for values of h_0/d_0 less than 0.13, implying that the influence of the initial still water depth, h_0, was minimal.

The Reynolds number was defined as $\mathrm{R} = V_m \cdot D_H/\nu$, where V_m is the depth-averaged profile velocity ("Velocity Profiles" section) and D_H is the hydraulic diameter. Values of $10^5 < \mathrm{R} < 10^6$ were obtained for all waves, which implied that a sufficient level of turbulence was ensured for both surges and bores, thus minimizing scale effects (Pfister and Chanson 2012). Similar results were presented by Wüthrich et al. (2016b).

The time origin was set as the opening time of the pipes, identified when a reduction in water elevation in the upper reservoir was measured. The wave arrival time at a specific location was set when a local wave height, h, greater than 0.01 m was recorded.

The repeatability of both surges and bores was investigated, and the representative results of the wave heights are presented in Fig. 6. For both wet and dry bed scenarios, the flow depth was measured at US7, which was located 13.85 m from the channel inlet. Wave profiles were normalized using the impoundment depth, d_0, and the dimensionless time, $T \cdot (g/d_0)^{0.5}$. Results showed similar profiles for all tests, with values of normalized standard deviation, σ/d_0, of less than 5% for wet bed bores and less than 3% for dry bed

Table 2. Experimental Program and Characteristics of the Performed Tests

Bed condition	Initial water depth [h_0 (m)]	Number of pipes	Equivalent impoundment depth [d_0 (m)]	h_0/d_0	Bore Froude $F_B = \frac{U}{\sqrt{gh_0}}$	Number of repetitions	Test number
Dry	0.000	3	0.82	—	—	8	1
		2	0.63	—	—	2	2
		1	0.40	—	—	2	3
Wet	0.001 (humid)	3	0.82	0.0012	—	1	4
	0.010	3	0.82	0.0122	9.85	3	5
		2	0.63	0.0159	8.62	2	6
		1	0.40	0.0250	6.67	2	7
	0.030	3	0.82	0.0366	5.22	4	8
		2	0.63	0.0476	4.61	2	9
		1	0.40	0.0750	3.60	2	10
	0.050	3	0.82	0.0610	3.93	5	11
		2	0.63	0.0794	2.49	2	12
		1	0.40	0.1250	2.74	2	13
	0.100	3	0.82	0.1219	2.69	1	14
Maximum	0.100	3	0.82	0.1219	9.85	8	—
Minimum	0.000	1	0.40	0.0012	2.49	1	—

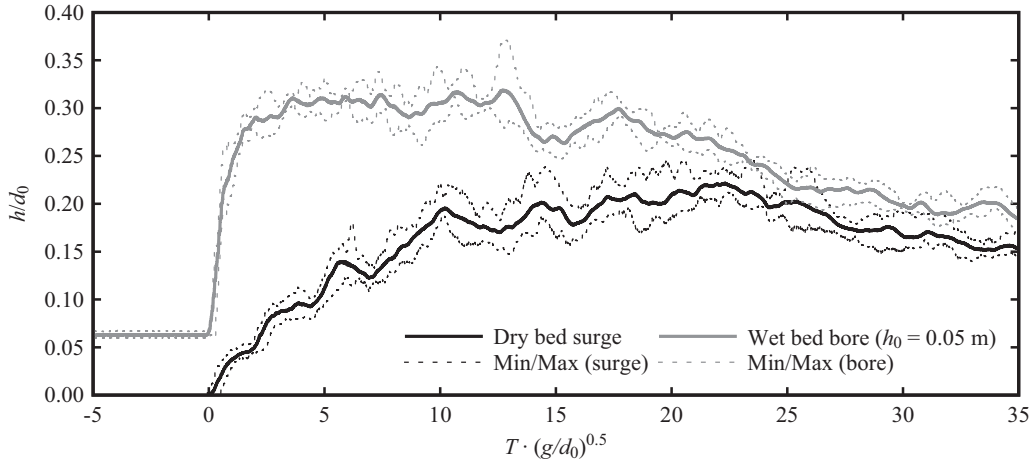

Fig. 6. Repeatability for dry bed surges (three pipes, d_0 = 0.82 m, Test 1, eight repetitions) and wet bed bores with three pipes, (three pipes, d_0 = 0.82 m, h_0 = 0.05 m, Test 11, five repetitions) measured at x of 13.85 m (US7)

surges. These results are similar to those of Shafiei et al. (2016) for bores. Some differences were observed in terms of surface turbulence; however, oscillations remained within the same range, and the spectral distribution of oscillating frequencies was similar for all tests (Wüthrich et al. 2016b).

The bidimensionality of both bores and surges was validated by measuring the wave profiles at two locations in the transversal axis of the channel at the same distance, x, of 13.60 m from the channel inlet (not shown). Fig. 7 presents a visual impression of the bidimensionality for both surges and bores.

Water Surface Profiles

The main characteristics of dry bed surges and wet bed bores produced with the vertical release technique are discussed in this section. For both surges and bores, water surface profiles were measured using seven USs located along the longitudinal axis of the channel (Fig. 3). The synchronization of the acquisition system allowed for the combination of all data and for the obtainment of a spatial-temporal evolution of the depth profile. In the following sections, the surges and bores generated with the vertical release technique are described and compared to the dam-break waves propagating on dry and wed beds in light of some of the relevant literature.

Dry Bed Surges

The propagation of the surge on the dry smooth channel visually appeared as a thin water layer followed by a continuous rise in water depth until a maximum value was reached. Subsequently, the water level started to decrease. The surge front propagated uniformly, and visually, little to no aeration was observed, as shown in Fig. 7.

The temporal development of the height of a specific surge (d_0 = 0.82, Test 1) propagating over a dry bed with a flat, smooth surface is presented in nondimensional form in Fig. 8. Each curve corresponds to a measurement location, with US7 located farthest downstream (Fig. 3). A decrease in the maximum depth was observed as the surge propagated along the channel. This decrease was

attributed to the viscous and diffusive behaviors of the flow. The similarity of the profiles farther downstream in the channel ($x > 10$ m) indicated that the surge was fully developed and that a quasi-uniform condition was reached. The observed surface fluctuations were secondary waves attributed to the turbulence of the flow (Wüthrich et al. 2016b). Some oscillations of the free surface due to the releasing mechanism were observed in the upstream section of the channel at $0 < x < 2$ m. However, they disappeared after the wave traveled a few meters farther downstream from the channel inlet.

The longitudinal water surface profiles, observed when the surge reached the locations, denoted as x, of 13.60 and 13.85 m (US6 and US7), were obtained for multiple dry bed surges under identical initial release conditions. The seven water depth measurement locations along the channel (Fig. 3) allowed for the obtainment of multiple data sets that were compared with the theoretical parabolic profile from Ritter (1892) presented in Eq. (2). The experimental points are shown in Fig. 9 using the nondimensional streamwise displacement defined as $x/[t \cdot (gd_0)^{0.5}]$.

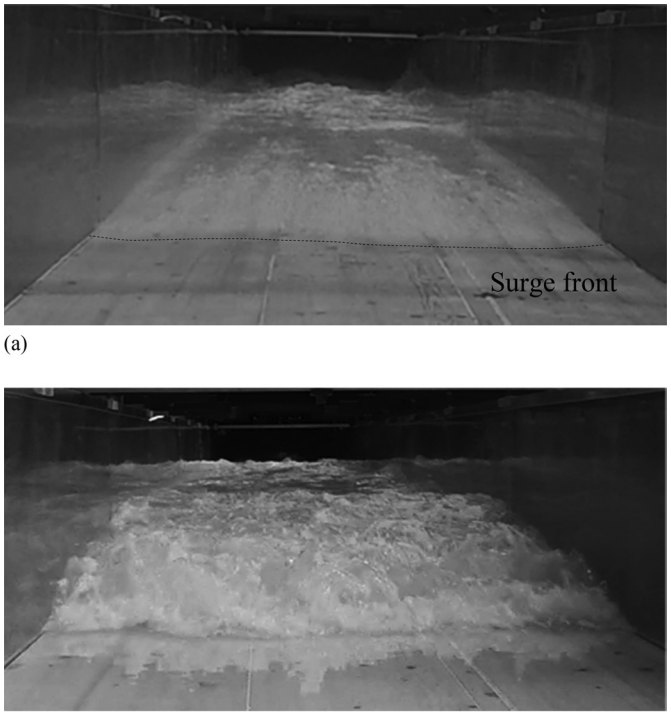

(a)

(b)

Fig. 7. (a) Front of the surge propagating over dry bed (3 pipes, d_0 = 0.82 m, Test 1); (b) wet bed bore (d_0 = 0.82 m, h_0 = 0.05 m, Test 11) with its turbulent front. (Images by Davide Wüthrich, May 2014.)

$$\frac{h}{d_0} = \frac{1}{9} \cdot \left(2 - \frac{x}{t \cdot \sqrt{gd_0}}\right)^2 \tag{2}$$

Although some minor scattering was found in the upstream part of the surge due to water surface fluctuations, good agreement between all tests was observed. A marginal variation occurred in the tip region for scenarios with different d_0 values because of the different propagating velocities.

Fig. 10 presents a focus on the tip region, where the higher densities of USs allowed for a more precise investigation of the tip shape. The experimental points obtained for multiple surges with different impoundment depths, denoted by d_0, measured at various channel locations, were compared with the theoretical solutions of Whitham (1955) in

$$\frac{x - x_s}{d_0} = -\frac{f}{8} \cdot \frac{U^2}{g \cdot d_0} \cdot \left(\frac{g}{\partial U/\partial t}\right)^2 \cdot \left[ln\left(1 + \frac{8}{f} \cdot \frac{h/d_0}{U^2/(g \cdot d_0)} \cdot \frac{\partial U/\partial t}{g}\right) + \frac{8}{f} \cdot \frac{h/d_0}{U^2/(g \cdot d_0)} \cdot \frac{\partial U/\partial t}{g}\right] \tag{3}$$

where f = friction factor of 0.021; U = front celerity of 3.56 m/s for a d_0 value of 0.82 m; and $\partial U/\partial t$ = 0.15 m/s^2. The latter was calculated from the linear interpolation of the average velocity profiles obtained from the UVP measurements. Good agreement was also found with the theoretical solution of Chanson (2009) for the same friction factor (f).

$$\frac{h}{d_0} = \sqrt{\frac{f}{4} \cdot \left(\frac{U}{\sqrt{gd_0}}\right)^2 \cdot \left(\frac{x - x_s}{d_0}\right)} \tag{4}$$

where x_s = location of the front. The results are presented in Fig. 10, where good agreement between all data and curves was observed, indicating consistency with the literature. Furthermore, the experimental points were also compared to prototype points

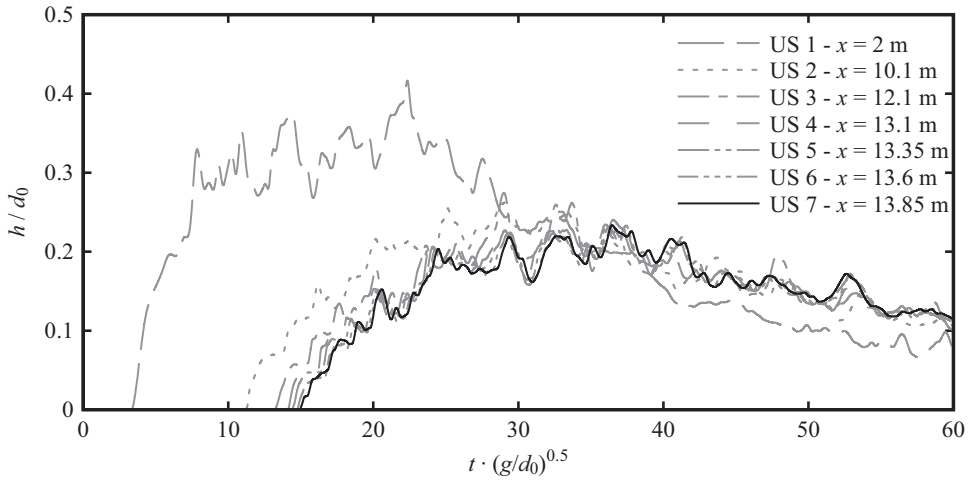

Fig. 8. Evolution of the surge on dry bed with d_0 of 0.82 m for Test 1

J. Waterway, Port, Coastal, Ocean Eng., 2018, 144(4): 04018006

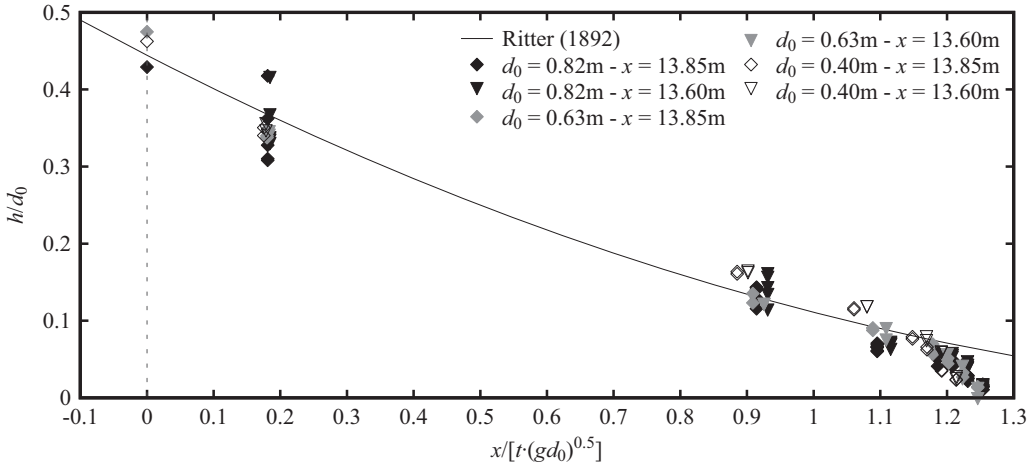

Fig. 9. Longitudinal dimensionless water surface profiles when the wave reached two measurement locations, at x = 13.60 and 13.85 m for US6 and US7, respectively; comparison of all generated surges with d_0 values of 0.82, 0.63, and 0.40 m with the theoretical solutions from Ritter (1892)

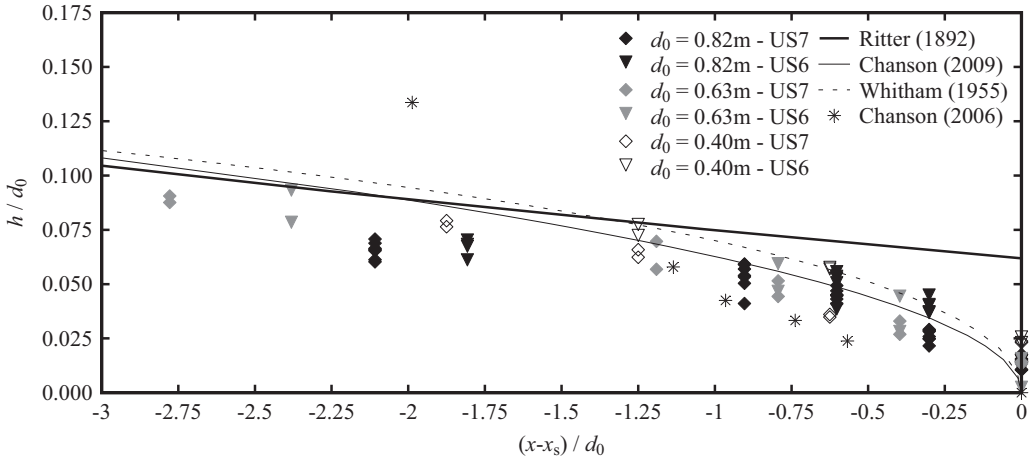

Fig. 10. Comparison of the measured longitudinal wave profiles with the theoretical solutions of Ritter (1892), Whitham (1955), Chanson (2009), and prototype data (Chanson 2006) in the wave-tip region where x was 13.85 and 13.60 m for US7 and US6, respectively

derived from a propagating tsunami-induced inundation advancing inland during the 2004 Indian Ocean Tsunami (Chanson 2006). The good agreement observed in Fig. 10 indicates that the dry bed surges generated with the vertical release technique were representative of the overland flow of real tsunamis observed during such events.

Wet Bed Bores

The difference between dry bed surges and wet bed bores was evident in Fig. 2. On visual appearance, the propagating bore was similar to a turbulent and highly aerated hydraulic jump [Fig. 7(b)] with periodic surface fluctuations in the form of lumps being ejected and with significant air entrainment observed in the front region. Similar observations were described by Leng and Chanson (2015) for positive surges and tidal bores (Fig. 2). According to Yeh and Mok (1990), the front roller was formed by the flow separation initiated at the front toe resulting from the streamline divergence caused by the sudden raise in water depth. Furthermore, the same authors observed a *generation-advection cycle*, suggesting that the eddies formed inside the roller were later advected in the flow where turbulence stretching in the slanting vertical direction was detected (Yeh and Mok 1990). Air was entrained behind the bore front for a length of L_r, where air bubbles could be observed, whereas farther behind, mainly clear water appeared.

The development of a wet bed bore propagating over a still water depth, h_0, was investigated at different locations along the longitudinal axis of the channel, and the time-history of the water surface is presented in Fig. 11 for a specific case (d_0 = 0.82 m, h_0 = 0.05 m, Test 11). A substantial difference in behavior from dry bed surges was observed for bores because of a sudden rise in water height at the front. For all wet bed bores, a temporal conservation of maximum depth was observed during propagation along the channel. This conserved depth resulted in a uniform translation of the bore shape.

The influence of the initial still water depth, h_0, on the propagating bore (Fig. 3) was investigated by testing different h_0 values ranging between 0.001 and 0.1 m (Table 2), where the lower value represented a bore propagating over a thin water layer remaining from a previous test. Multiple impoundment depths, denoted by d_0, were tested, resulting in ratios of $0.0012 < h_0/d_0 < 0.1219$ (Table 2). Similar to those of Chanson et al. (2003) and Nouri et al. (2010), the

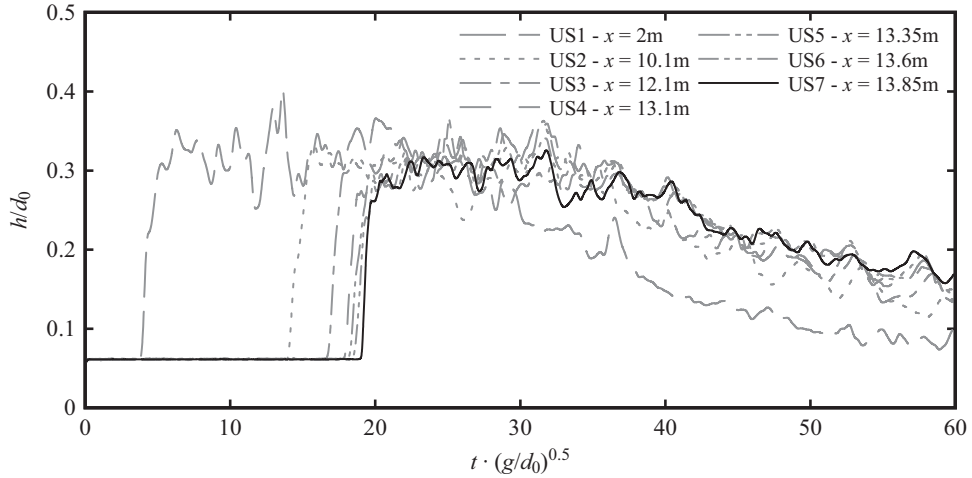

Fig. 11. Time evolution of a bore on wet bed ($d_0 = 0.82$ m, $h_0 = 0.05$ m, Test 11) at different locations along the longitudinal axis of the channel

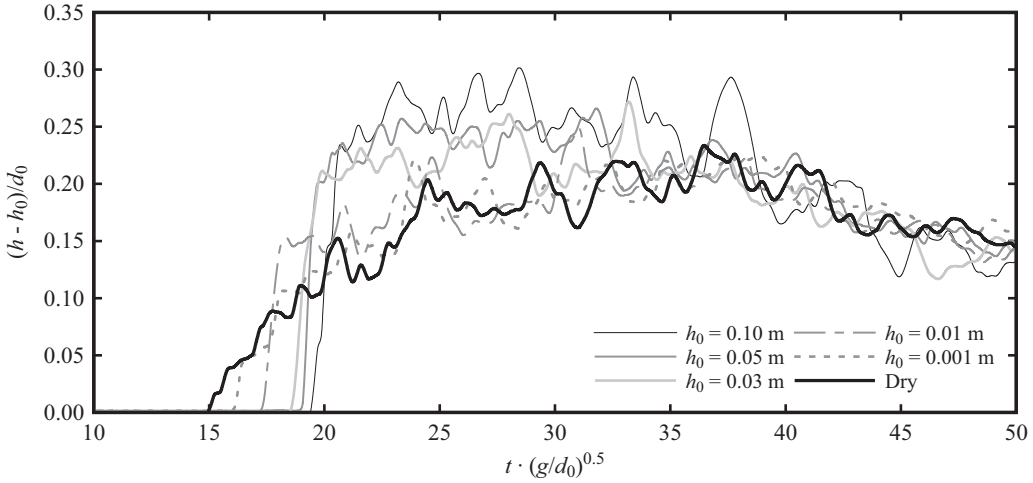

Fig. 12. Bore profiles for waves with different initial still water depths at x of 13.85 m (US7) for d_0 of 0.82 m with all profiles brought down to $(h–h_0)/d_0$ for Tests 1, 4, 5, 8, 11, and 14

results showed that, even for a thin still water layer, the properties of the propagating bore were different from those of a dry bed surge. For still water heights greater than 0.03 m, similar profiles were measured, suggesting that beyond this value, h_0 had less influence. For decreasing initial still water depths ($h_0 < 0.03$ m), a transitional bore, with behavior that became more similar to that of a dry bed surge with milder front steepness, was observed (Fig. 12). The shift in arrival time revealed different bore front celerity magnitudes that depended on the initial still water depth, h_0.

As previously discussed by Stoker (1958), the temporal evolution of a dam-break bore propagating over a wet bed can be divided into four main regions (downstream to upstream): (1) the turbulent bore front; (2) a *plateau*, which is a region with almost constant water height, h_2; (3) a far back region where the Ritter (1892) theory for a surge propagating on a dry bed can be applied; and (4) the upstream reservoir where h is equal to d_0. Fig. 13 presents, for all experimental tests, the longitudinal profiles of the water surface (arrival time was defined when a threshold of $h = h_0 + 0.01$ m was registered at US7, x = 13.85). These profiles were also successfully compared with those of Ritter (1892) in the far back region and with those of Stoker (1958) for dam-break waves propagating over a wet bed with zero initial velocity in both the upstream and downstream reservoirs. The good agreement observed in Fig. 13 proves that, similar to previously shown surges, the vertical release technique produced bores that were comparable to those of the classical dam-break scenario. The height of the plateau region (h_2, horizontal lines in Fig. 13) was predicted using the numerical approximation deduced from the continuity and momentum equations in Eq. (5) (Chanson et al. 2000) and compared to the experimental points in Fig. 14.

$$\frac{h_2}{d_0} = 0.932\left(\frac{h_0}{d_0}\right)^{0.371} \tag{5}$$

Fig. 14 shows that, for all performed tests, the ratio h_0/d_0 was lower than the critical h_0/d_0 value of 0.138, implying that the initial discharge, Q_0, was independent of the initial water depth, h_0.

As shown in Fig. 15, for all tests performed on the wet bed and for all values of h_0 and d_0, the shape of the bore front was normalized using h_2 and the roller length, L_r, and good agreement between

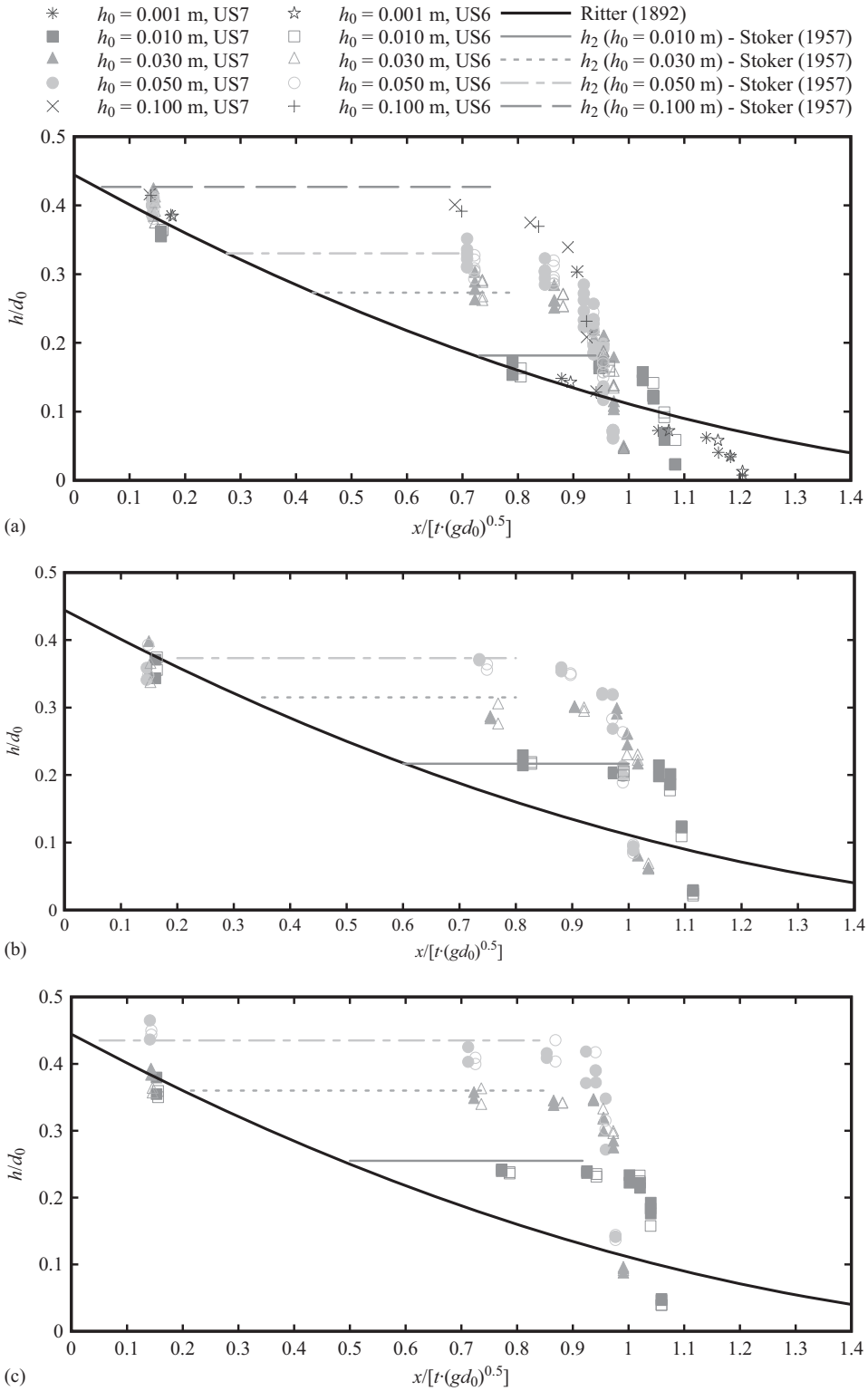

Fig. 13. Longitudinal free-surface profile for bores with different initial still water depths, denoted h_0, and impoundment depths, denoted d_0, compared with the theoretical solutions of Ritter (1892) and the plateau heights, denoted h_2, obtained with Eq. (5) (Chanson et al. 2000); measurements at US 7 (solid symbols) and US 6 (empty symbols): (a) $d_0 = 0.82$ m; (b) $d_0 = 0.63$ m; (c) $d_0 = 0.40$ m

all curves was observed. Given the differences in front celerity and flow depth, the length of the roller L_r was identified for every profile using the time taken by the bore to reach the plateau height of h_2. The roller length L_r was then derived using the bore celerity such that L_r was $U{\cdot}t$. The experimental results were successfully compared to formulas found in the literature, and the longitudinal free-surface elevations showed a self-similar profile in the form of Eq. (6). For the present study, the best fit was found with the exponent, $N = 0.482$ which was located between the N value of 0.441 proposed by Chanson (2011) for hydraulic jumps and the N value of 0.540 suggested by Wang and Chanson (2015). Eq. (6) is written as

J. Waterway, Port, Coastal, Ocean Eng., 2018, 144(4): 04018006

$$\frac{h - h_0}{h_2 - h_0} = \left(\frac{x - x_s}{L_r}\right)^N \quad (6)$$

Flow Velocities

Front Celerity

Two velocities were analyzed in the present study: (1) the surge and bore front celerity values, denoted U, derived from the spatial-temporal advancement of the wavefront as detected by the USs and (2) the velocity profiles within the wave as measured using the ultrasonic velocity profilers (UVP).

The average front celerity of the propagating wave was estimated using the measurements of the depth profiles over time as follows:

$$U = \frac{\Delta x}{\Delta t} \quad (7)$$

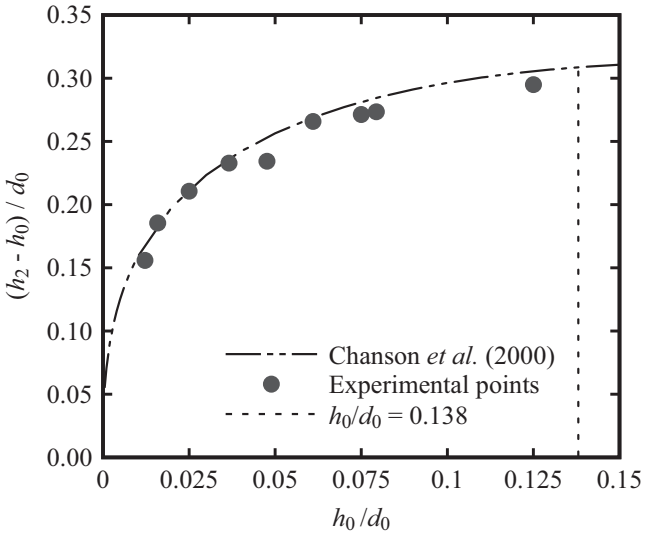

Fig. 14. Comparison of the experimental points of the plateau height, h_2, with the approximation proposed by Chanson et al. (2000) [Eq. (5)]

where Δx = distance between two USs; and Δt = difference in the wavefront arrival time. The measurement locations corresponded to the locations of the USs as shown in Fig. 3. The average front celerity was considered for each sensor (US2–US7) relative to US1, which was located at an x of 2 m from the channel inlet. The average front celerity obtained for dry bed surges was compared to formulas commonly used in design codes and practice (Fig. 16); these formulas were mostly derived from physical models at laboratory scale. This comparison proved that the waves generated with the proposed vertical release technique had celerity values consistent with other generation mechanisms described in literature. The celerity range was confined by values obtained from the FEMA 55 (upper bound) and the City and County of Honolulu (CCH) building code (lower bound) (FEMA 2001; CCH 2000). The experimental results obtained for the present study were between those of Kirkoz (1983) and Iizuka and Matsutomi (2000). Given the Froude similitude, most formulas estimating the velocities are expressed as

$$U = \alpha\sqrt{g d_0} \quad (8)$$

where α = coefficient for which the values are presented in Table 3. For the present study, the best correlation was found for an α value of 1.25 for dry bed surges (Fig. 16).

For the same release conditions, wet bed bores propagated with a slower front celerity compared to dry bed surges. This difference in behavior can be observed in Fig. 2 for the case of a tidal bore, where the portion of the wave on the dry bed propagated faster than the portion propagating over the wet bed. The front celerity, U, of a bore moving over a wet bed was a function of the initial still water depth, h_0, and small values of h_0 corresponded to velocities close to those observed for the dry bed condition, which represented the upper limit.

The experimental wavefront celerity, U, obtained for the wet bed bores with various values of h_0 and d_0 was compared with a theoretical solution derived from the momentum equation [Eq. (9)], as presented by Stoker (1958) and with the empirical approximation of Montes (1998), presented by Chanson (2004) in Eq. (10):

$$\frac{U}{g h_0} = \sqrt{\frac{1}{8} \cdot \left[\left(2\frac{h_2}{h_0} + 1\right)^2 - 1\right]} \quad (9)$$

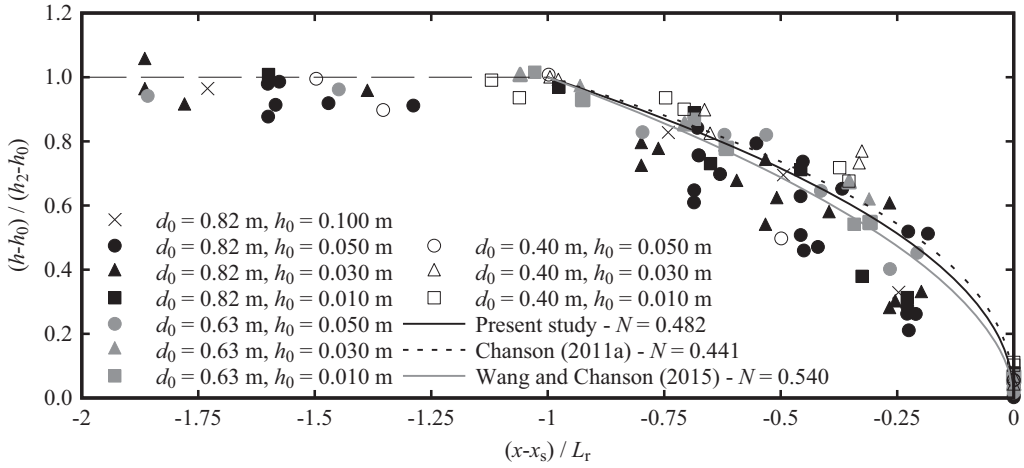

Fig. 15. Normalized bore front profiles, for various values of d_0 and h_0, for comparisons of the experimental data from the proposed vertical release technique with data from the empirical formulas from Chanson (2011) [Eq. (6)] and from Wang and Chanson (2015) for hydraulic jumps

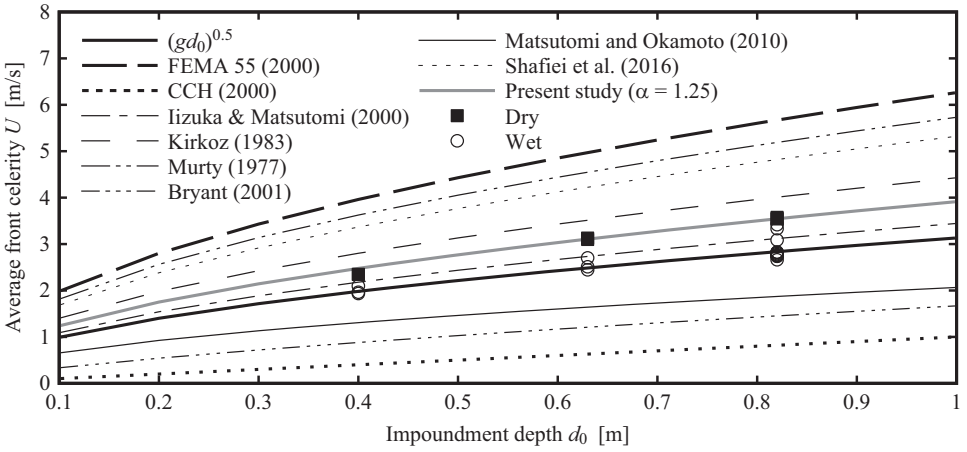

Fig. 16. Comparison of the measured average front celerity, U, with formulas from the literature for dry bed surges (all values at model scale)

Table 3. Coefficient α in Eq. (8)

Reference	α
Iizuka and Matsutomi (2000)	1.1
Kirkoz (1983)	$\sqrt{2}$
FEMA 55 (FEMA 2001)	2
Murty (1977)	1.83
Bryant (2001)	1.67
Matsutomi and Okamoto (2010)	0.66
Shafiei et al. (2016)	1.7
Present study	1.25

$$\frac{U}{\sqrt{gh_0}} = \frac{0.63545 + 0.3286\left(\frac{h_0}{d_0}\right)^{0.65167}}{0.00251 + \left(\frac{h_0}{d_0}\right)^{0.65167}} \tag{10}$$

where d_0 = initial equivalent impoundment depth; h_0 = initial still water depth; and h_2 = plateau height obtained from Eq. (5) and shown in Fig. 3. Very good agreement between all formulas can be observed in Fig. 17. This finding shows that, contrary to dry bed surges, for wet bed bores, a precise prediction of the front celerity can be achieved through Eqs. (9) and (10).

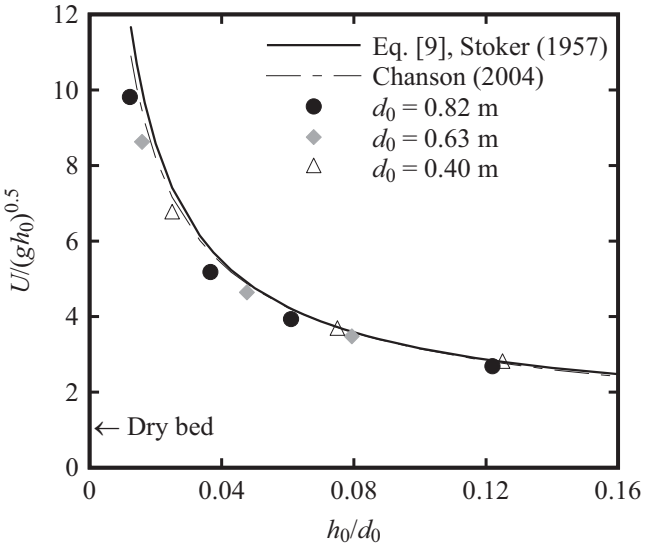

Fig. 17. Average bore front celerity, U, as a function of the initial still water depth, h_0; experimental results compared to the momentum equation [Eq. (9)] and the numerical approximation proposed by Chanson (2004), shown in Eq. (10), for different impoundment depths: d_0 was 0.82 m for Tests 4, 5, 8, 11, and 14; d_0 was 0.63 m for Tests 6, 9, and 12; and d_0 was 0.40 m for Tests 7, 10, and 13

Velocity Profiles

In addition to the recent contributions of Leng and Chanson (2017a, b), only a few studies of the in-wave velocity profiles were available. For this reason, a constant vertical velocity profile was commonly assumed (Whitham 1955).

Similar to the process described by Meile et al. (2008, 2011), a UVP probe installed in the channel bottom measured the internal instantaneous velocity profiles of the propagating surge and bore. Some representative velocity profiles are shown in Fig. 18, which presents the typical profiles associated with turbulent open channel flows. A well-defined boundary layer, followed by an upper sector with almost constant velocities were observed. These results confirmed that surges traveled faster than bores.

For all profiles, the depth-averaged velocity, V_m, was computed as

$$V_m = \frac{1}{h}\int_0^h v\, dh \tag{11}$$

where v = local velocity at depth h. The time history of V_m in Fig. 18 was compared to the wavefront celerity U measured with the USs. Looking at the depth-averaged velocity profiles, it is noticed that the largest velocities occurred at the wavefront, which was consistent with other reports in the literature. A continuous deceleration occurred behind the wavefront for all configurations until a quasi-steady state was reached (not discussed herein): This was previously reported by Al-Faesly et al. (2012) and Goseberg et al. (2013). Although the observed deceleration behind the wavefront was predicted by the continuity equation because of the increase in water depth, the last part of the curve was influenced by the

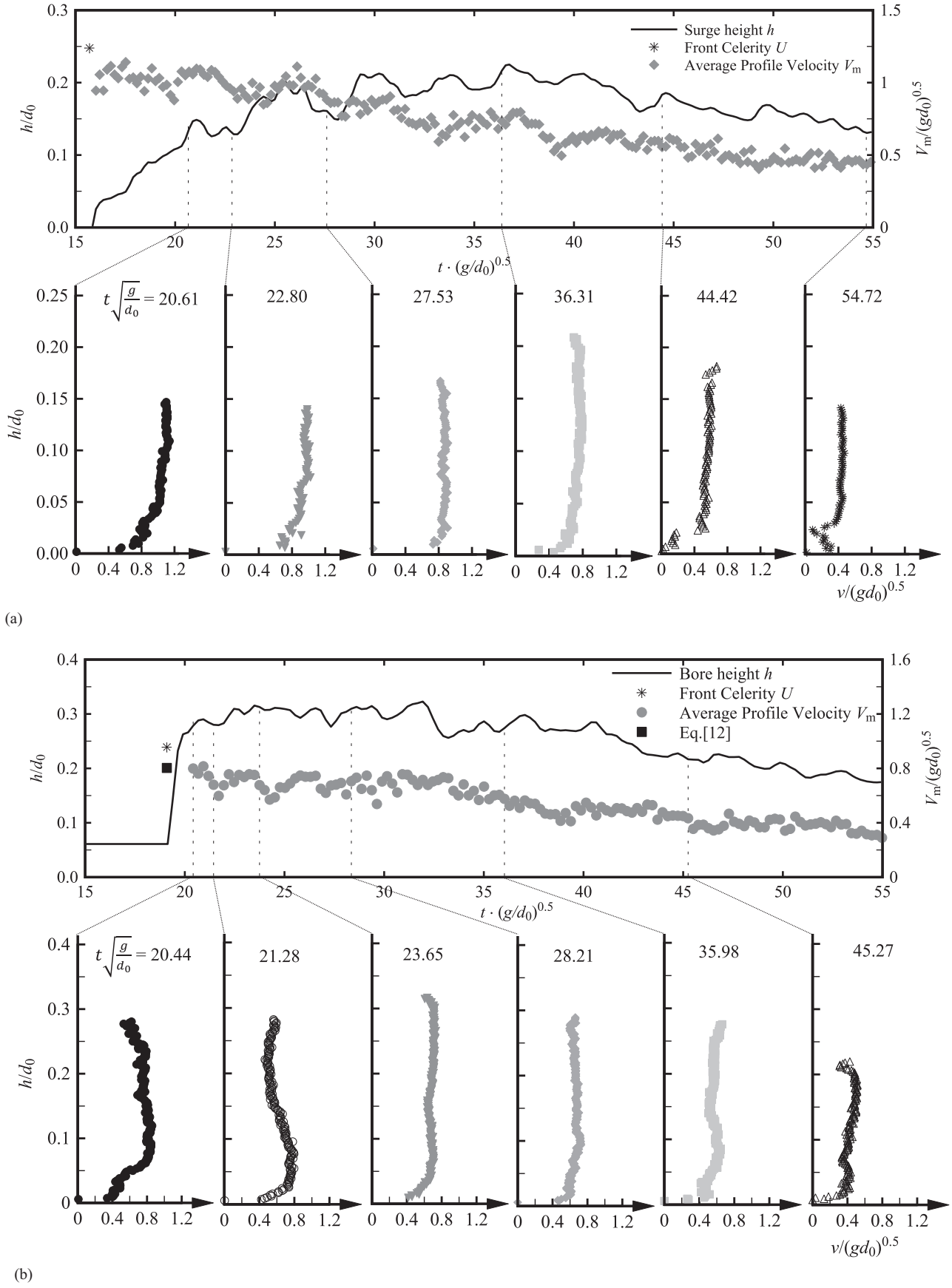

Fig. 18. Wave height, h, depth-averaged velocity, V_m, and velocity profiles at specific times for (a) dry bed surge with $d_0 = 0.82$ m for Test 1 and (b) wet bed bore with $d_0 = 0.82$ m and $h_0 = 0.050$ m for Test 11, both measured at x of 13.85 m (US7) from the channel inlet

J. Waterway, Port, Coastal, Ocean Eng., 2018, 144(4): 04018006

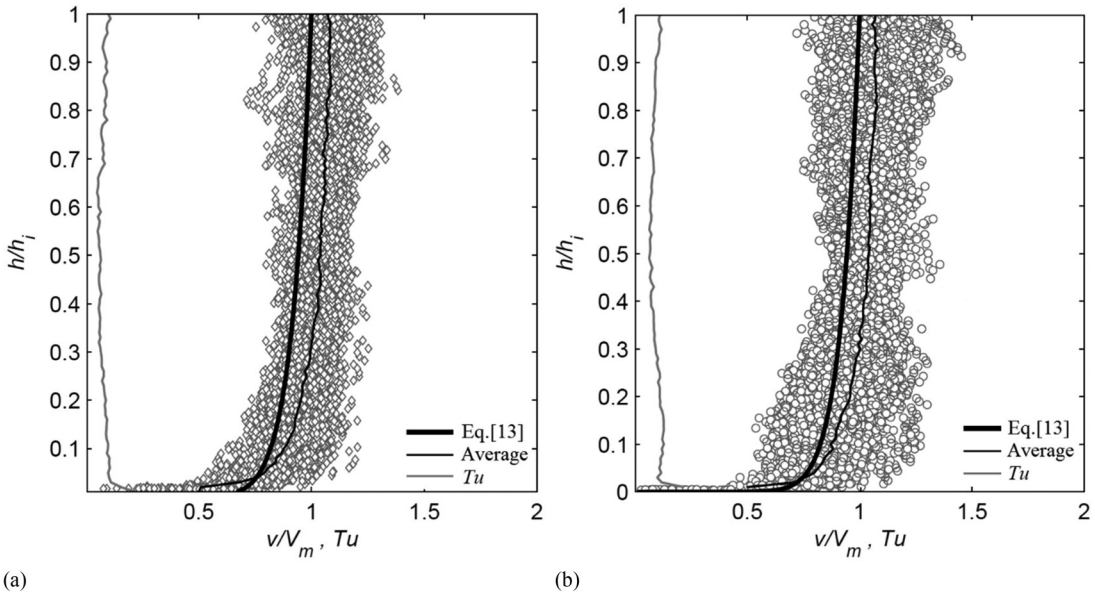

Fig. 19. Normalized velocity profiles and turbulent intensity, Tu, for $T{\cdot}(g/d_0)^{0.5} < 42$: (a) dry bed surge (160 profiles Test 1); (b) wet bed bore with $d_0 = 0.82$ m and $h_0 = 0.05$ m (104 profiles, Test 11)

reduction of the water volume, and implicitly, of the hydraulic head in the upper basin. For these reasons, all data for T greater than T^* were not considered.

The lower velocities observed after the passing of the wavefront were in agreement with the findings of Lauber and Hager (1998) and those of Leng and Chanson (2016, 2017b). In Fig. 18, for bores, the experimental data were also compared with the velocity V_2 behind the bore front predicted by the following momentum equation (Henderson 1966; Chanson 2004):

$$U \cdot h_0 = (U - V_2) \cdot h_2 \tag{12}$$

where U = bore front celerity; h_0 = initial still water depth; and h_2 = bore height after the turbulent front [Eq. (5)].

All individual velocity profiles were normalized using the measured depth-averaged velocity, V_m, and the wave height of every profile, h_i. Although the profiles showed some scattering, probably attributable to random air bubbles or impurities occurring in the flow, good agreement between all measured profiles for a dry bed surge and a wet bed bore can be observed in Fig. 19. The velocity profiles were successfully compared to Prandtl's power law with n of 8, obtained with a flow resistance value f of 0.02 (Chanson 2004):

$$\frac{h}{h_i} = \left(\frac{V}{V_m}\right)^n \tag{13}$$

Although a logarithmic profile, which takes into account the velocity reduction close to the bottom due to the presence of the boundary layer, is theoretically more appropriate, Fig. 19 shows that the assumption of a uniform constant velocity profile was feasible for both dry bed surges and wet bed bores. This can be explained by the significant vertical exchange of momentum across the wave depth due to turbulence. The estimation of the average velocity through a uniform profile works well in the fully developed region, where the height of the flow is sufficient to neglect the effect of the boundary layer. In the tip region, the thickness of the boundary layer is important; hence, V_m is slightly underestimated. The existence of a thin boundary layer was previously observed by Lauber and Hager (1998) through particle image velocimetry (PIV) tests; however, this was small given the range of Reynolds numbers ($\mathrm{R} \approx 10^5$–10^6). The same findings were confirmed by Leng and Chanson (2017a, b) for surges and bores in both steady and unsteady flows. Some scattering in velocity measurements was visible in the upper part of the profiles (Fig. 19), which was probably attributable to the fluctuations observed on the flow surface (Wüthrich et al. 2016b). To gain a better insight into the turbulent behavior of the surges and bores, the fluctuations were separated from the mean values and analyzed per horizontal flow layer. This process resulted in a turbulence intensity value, $Tu = \sqrt{\overline{(v-\bar{v})^2}}/\bar{v}$, per layer. The derived Tu distribution is also presented in Fig. 19 and shows a uniform behavior with Tu values less than 0.11 for dry bed surges and less than 0.13 for wet bed bores. Similar results were obtained for other surges and bores with different values of impoundment depth, d_0, and initial still water depth, h_0.

The depth-averaged velocities, designated by V_m, for 12 dry bed surges and 19 wet bed bores at two measurements locations along the channel (x was 10.20 and 13.85 m) are presented in dimensionless form in Fig. 20, where $T = t - t_0$ is the shifted time, such that $T = 0$ coincides with the wave arrival time. The profile plotting was stopped when T equaled T^* because the assumption of a continuous water discharge, Q_0, was no longer valid (Fig. 5). Despite some scattering, good agreement was observed for all experimental points for both dry bed surges and wet bed bores. For dry bed surges, the match between the front celerity and depth-averaged velocity was good, whereas for bores on a wet bed, an underestimation of the velocity magnitude was consistently observed in the wavefront region [$T{\cdot}(g/d_0)^{0.5} < 15$, in Fig. 20(b)]. In this region, V_m was equal to the velocity V_2, derived from the momentum equation [Eq. (12)] as a function of h_0/d_0. For both surges and bores, the decrease in V_m behind the front was best approximated by Eq. (14), which imposed the boundary condition $V_m = U$ at $T{\cdot}(g/d_0)^{0.5} = 0$:

$$\frac{V_m}{U} = 1 - c \cdot \tanh\left[b \cdot T\sqrt{\frac{g}{d_0}}\right] \tag{14}$$

where V_m = depth-average profile velocity; U = wavefront celerity; T = shifted time ($T = t - t_0$); g = gravity constant; and d_0 = initial impoundment depth. Parameters b and c were derived empirically.

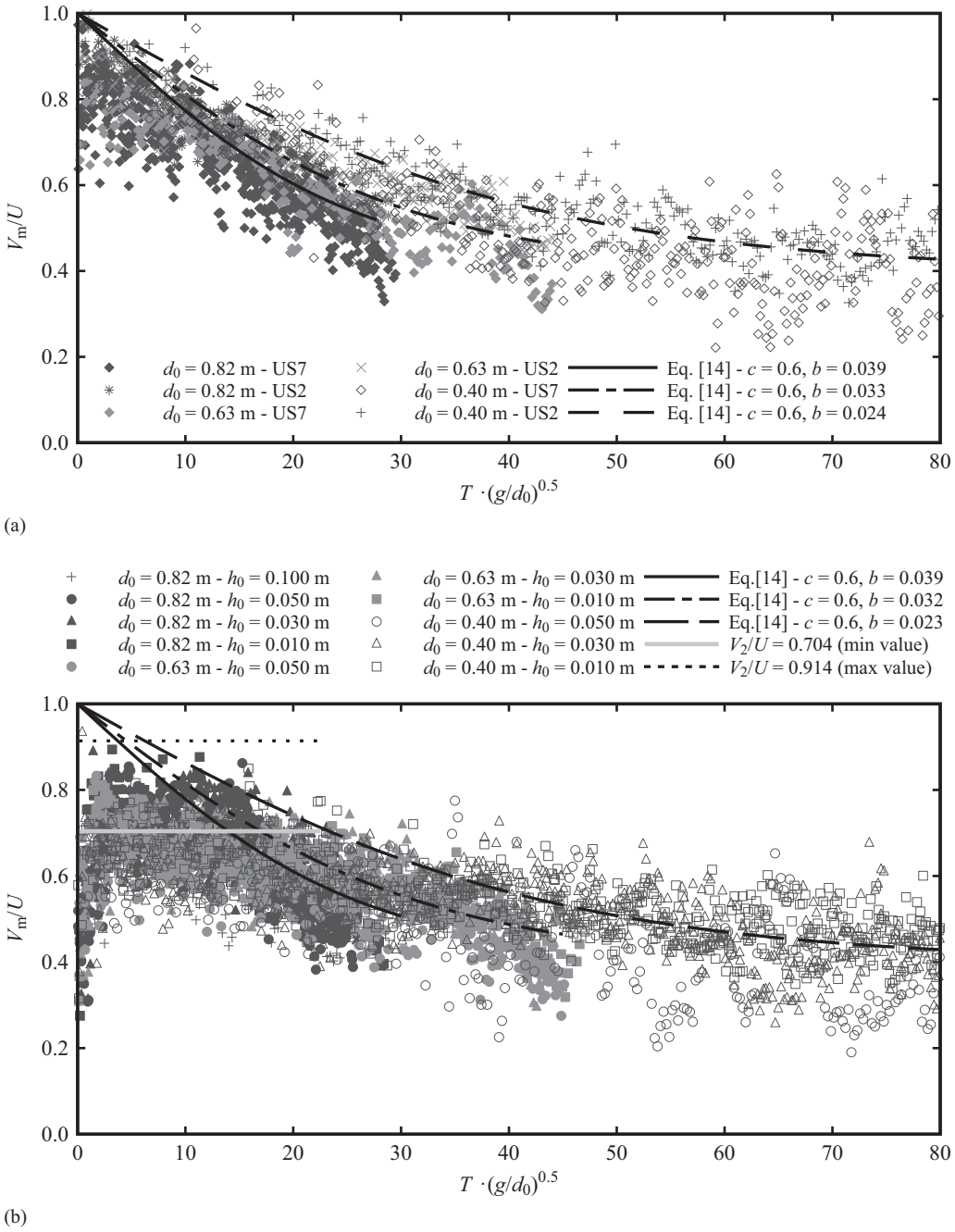

Fig. 20. (a) Dimensionless depth-averaged velocities, V_m/U, for 12 dry bed surges with different impoundment depths at two different locations at x of 13.85 and 10.20 m for US7 and US2, respectively; (b) dimensionless depth-averaged velocities, V_m, for 19 wet bed bores with different impoundment depths and initial still water depths at a fixed location, x = 13.85 m

For large values of $T \cdot (g/d_0)^{0.5}$, asymptotic behavior toward uniform flow conditions was observed. While the c value of 0.6 was a constant for both bores and surges (empirical best fit), b was influenced by the equivalent impoundment depth, d_0, and the wave height, h, as shown in Fig. 21 and as follows in Eqs. (15*a*) and (15*b*):

$$\text{Dry bed surge } b = 0.0124 \cdot \left(\frac{d_0}{h_{\max}} - 1\right) \tag{15a}$$

$$\text{Wet bed bore } b = 0.0124 \cdot \left(\frac{d_0}{h_2 - h_0} - 1\right) \tag{15b}$$

where $h_{\max}$ = maximum wave height for a dry bed surge in Eq. (15*a*); and h_2 = plateau height for wet bed bores in Eq. (15*b*). For the latter, the value of b was implicitly influenced by the initial still water depth h_0 through the plateau height h_2, which was a function of the ratio h_0/d_0 [Eq. (5), Fig. 14]. However, Fig. 21(a) shows that this dependence was minimal, meaning that the main parameter controlling b was the impoundment depth d_0 [horizontal trend shown in Fig. 21(a)]. These findings showed that, within the tested range, the main influence of the initial still water depth, h_0, was observed in the reduction of the wavefront celerity, U ("Front Celerity" Section).

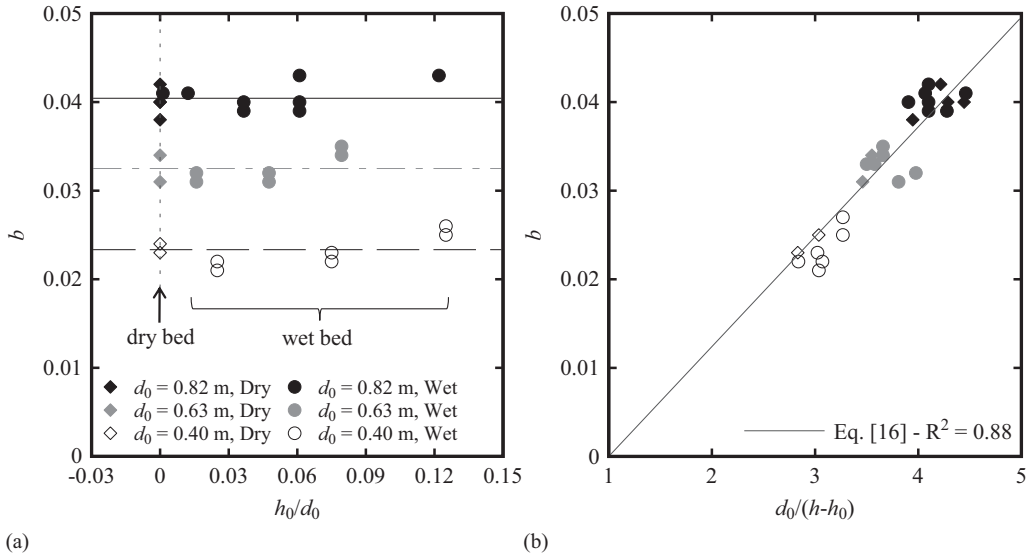

Fig. 21. Definition of parameter b in Eq. (15): (a) Eq. (15*a*) function of h_0/d_0; (b) Eq. (15*b*) function of $d_0/(h–h_0)$, where h equals h_{max} for surges and h equals h_2 for bores (Note: Same legend applies to both panels)

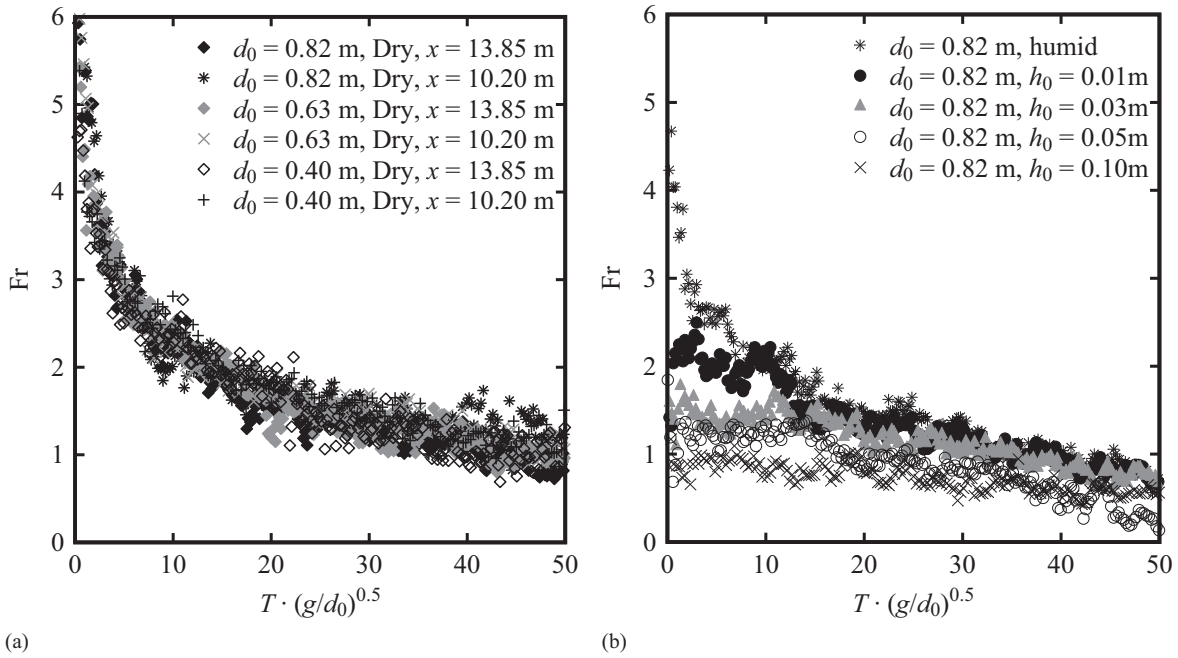

Fig. 22. Flow Froude number, F, computed for (a) dry bed surges and (b) wet bed bores

Froude Number and Momentum

The Froude number for both dry bed surges and wet bed bores was calcualted using Eq. (16) as follows:

$$\mathrm{F} = \frac{V_{m,i}}{\sqrt{g h_i}} \tag{16}$$

where V_m = individual depth-averaged profile velocity; g = gravity constant; and h_i = wave height of every profile. The values obtained are presented in Fig. 22, where a clear difference between bores and surges is shown. The dry bed surge was supercritical in the first part of the propagating wave, followed by an asymptotic decrease toward F ≈ 1. For wet bed bores, a more constant flow pattern was observed at all times. This between surges and bores difference was more important as h_0 increased. The behavior of wet bed bores with smaller initial still water depth, h_0, became similar to that of the dry bed surges. This proved, once again, the transition pattern between dry and wet beds. These findings were consistent with the video analysis of Fritz et al. (2012), who estimated Froude number values close to 1 in Kesennuma during the 2011 Tōhoku, Japan, tsunami.

The momentum associated with the moving wave was an important parameter because it directly controlled the loading exerted during the impact against a free-standing structure. The momentum, M, per unit width was calculated as the product of water density, ρ, unit discharge, q, and the average profile velocity, V_m, resulting in

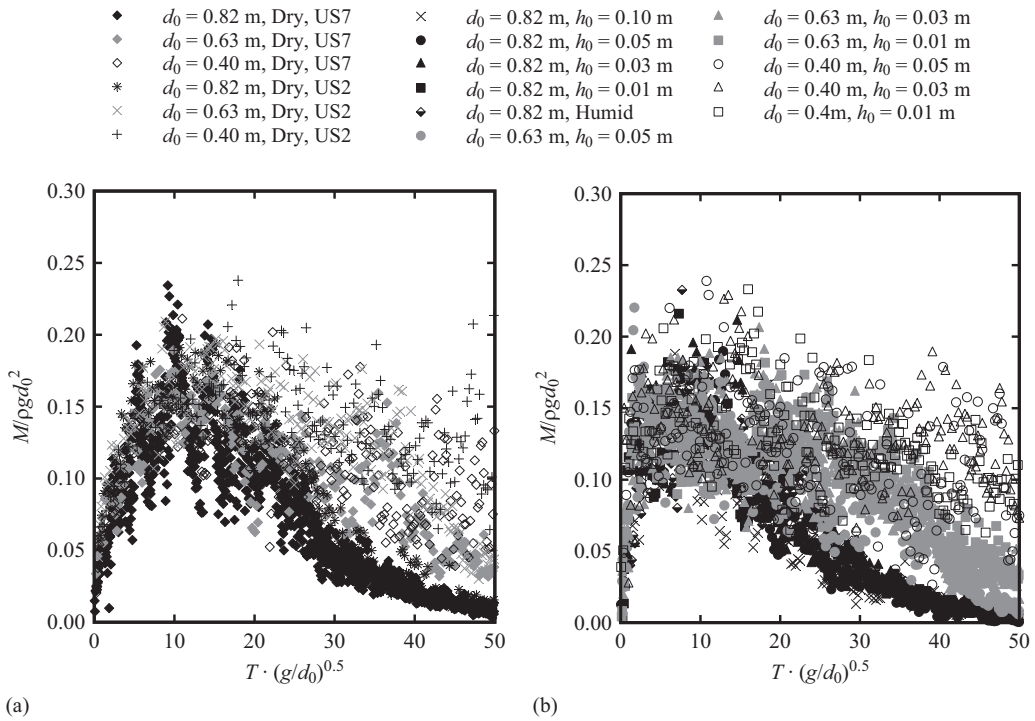

Fig. 23. Momentum, $M = \rho \cdot h \cdot V_m^2$, computed for (a) dry bed surges and (b) wet bed bores for various impoundment depths, denoted d_0, and initial still water depths, denoted h_0

$$M = \rho \cdot q \cdot V_m = \rho \cdot h \cdot V_m^2 \tag{17}$$

The results obtained from all tests are shown in Fig. 23, where a similar pattern between surges and bores can be observed, including the initial part characterized by an increase in momentum, followed by a subsequent decrease. Although some scattering was present, results showed a peak for all configurations around $T \cdot (g/d_0)^{0.5} \approx 10$, for which values of $M/\rho g d_0^2$ between 0.20 and 0.25 were obtained. It is noteworthy that the maximum of the momentum flux per unit width occurred neither when the velocity was maximal nor when the wave height was maximal, which is in agreement with findings previously reported by Yeh (2007) and Chock et al. (2013). For all tested scenarios, the maximum momentum was reached before the maximum flow depth was observed.

A variable h_M is introduced as the ratio between the height at which the maximum momentum occurs, $h(M_{\max})$, and the maximum wave height, $h_{\max}$, as

$$h_M = \frac{h(M_{\max})}{h_{\max}} \tag{18}$$

The results for both surges and bores are shown in Fig. 24. These findings were compared to those of Chock (2015), which showed that the maximum momentum occurred when the water level reached 67% of the maximum wave height recorded on the rising limb of the inundating wave. The approach by Chock (2015) is, on average, supported by the results for dry bed surges ($h_0/d_0 = 0$). However, discrepancies were observed for the case of wet bed bores; for these, given the sudden water rise of the water depth, the maximum momentum was observed when the water depth was approximately 90% of the maximum wave height. Thus, the chosen value of 67% may not be conservative for some cases and the maximum momentum might occur for higher water depths.

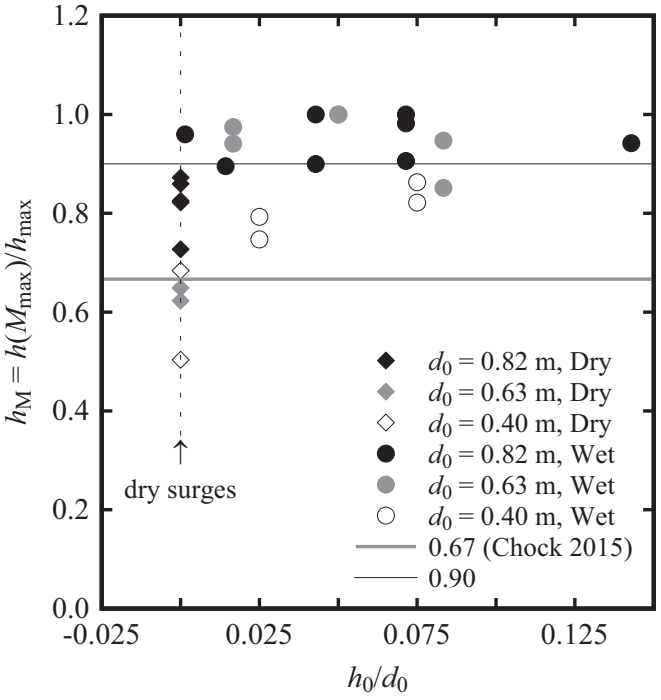

Fig. 24. Dimensionless surge and bore heights when maximum momentum occurred compared with existing guidelines ($h_M = 0.67$) by Chock (2015)

Discussion

The present study introduced a novel technique to generate dry bed surges and wet bed bores in a laboratory environment. If a 1:30

Froude scaling ratio was assumed, surge and bore depths ranged between 3.9 and 7.8 m (prototype scale), with front celerity values between 10.59 and 19.5 m/s. These values were consistent with field data obtained through posttsunami field surveys and observations, in which flow depths between 4 and 7 m were measured in the southern part of Khao Lak, Thailand, during the 2004 Indian Ocean tsunami (Dias et al. 2006) and velocities as high as 10–13 m/s near the Sendai Airport during the 2011 Tōhoku, Japan, tsunami (Jaffe et al. 2012). The generated surges and bores were similar to those produced with the classical dam-break technique (Ritter 1892; Whitham 1955; Stoker 1958), a method that is widely used at present to reproduce inland tsunami flows. Similarities between experimental and prototype data were also pointed out in terms of the shape at the surge front tip. Furthermore, similar Froude numbers between prototype and real tsunami events were presented. Thus, the authors concluded that the vertical released technique generates surges and bores that are consistent with other methods presented in literature and that this mechanism is well suited to simulate tsunami-like waves in laboratories.

Conclusions

Tsunamis, impulse waves, and dam-breaks waves are rare but highly destructive phenomena. Recent catastrophic events have shown that measures need to be taken to reduce casualties and socioeconomic impacts. The diversity of wave transformation and subsequent inland propagation has led researchers to develop several techniques to generate such tsunami-like flows in laboratories. This comprehensive study focused on the generation of long waves (surges and bores) through the vertical release of a stored water volume. Both surges and bores produced with this vertical release technique were then analyzed in terms of their hydrodynamic behavior and characteristics, and the following conclusions were drawn:

- A comparison with existing literature for the classical dam-break generation mechanisms showed good agreement between the dry bed surges generated by the proposed vertical release method and the analytical solutions of Ritter (1892) and Whitham (1955). For wet bed bores, the generated water surface profiles agreed well with the theory of Stoker (1958).
- The values of wavefront celerity were successfully compared to those found in the existing literature and the current design guidelines and codes. A new expression to compute wavefront celerity was proposed in Eq. (8) with an α coefficient of 1.25. For wet bed bores, very good agreement was found with the momentum equation [Eq. (9)] and the numerical approximation of Chanson (2004). The influence of the initial impoundment depth, h_0, was observed in the wavefront celerity U, whereas bores propagating over smaller initial still water depths, showed behavior similar to that of dry bed surges.
- The use of UVP probes allowed for the measurement of velocity profiles of the propagating wave behind the wavefront, which showed velocity profiles close to those observed in open channel flows. Although the normalized profiles indicated good agreement with Prandtl's exponential law, experimental results proved that the common assumption of a constant velocity profile over depth was acceptable. Flow deceleration was observed behind the front for all scenarios, and an expression to predict the depth-averaged velocity at a certain time behind the front was proposed in Eq. (14). The latter did not directly depend on the initial still water depth, h_0; rather, it depended on the equivalent impoundment depth, d_0.
- Dry bed surges exhibited higher Froude numbers in the wave tip region, followed by a rapid decrease, whereas wet bed bores showed more constant Froude numbers over time. All tests had a similar shape for the momentum profiles with maxima occurring at $T\cdot(g/d_0)^{0.5} \approx 10$, which did not correspond to either the maximum wave height or to the maximum flow velocity. The maximum momentum occurred at 65–70% of the maximum wave height for dry bed surges and at 90% of the maximum wave height for wet bed bores, something consistent with the latest standard recommendations (Chock 2015).

Acknowledgments

The authors thank Professor Hubert Chanson (University of Queensland, Australia) for his advice. The research study was supported by the Swiss National Science Foundation (SNSF) (Grants 200021_149112/1 and 200021_149112/2).

References

Al-Faesly, T., Palermo, D., Nistor, I., and Cornett, A. (2012). "Experimental modeling of extreme hydrodynamic forces on structural models." *Int. J. Protective Struct.*, 3(4), 477–505.

Allsop, W., Chandler, I., and Zaccaria, M. (2014). "Improvements in the physical modelling especially in the modelling of tsunamis and their effects." *Proc., 5th Int. Conf., Coastlab14: Application of Physical Modelling to Port and Coastal Protection*, V. Penchev and F. T. Pinto, eds., Black Sea—Danube Coastal Research Association, Varna, Bulgaria.

Arnason, H., Petroff, C., and Yeh, H. (2009). "Tsunami bore impingement onto a vertical column." *J. Disaster Res.*, 4(6), 391–403.

Blanckaert, K., and Lemmin, U. (2006). "Means of noise reduction in acoustic turbulence measurements." *J. Hydraul. Res.*, 44(1), 3–17.

Bryant, E. (2001). *Tsunami: The underrated hazard*, 1st Ed., Cambridge University Press, New York.

CCH (City and County of Honolulu). (2000). "City and County of Honolulu building code." *Chapter 16, Article 11*, Honolulu, HI.

Chandler, I. D., Allsop, W. H., Barranco Granged, I., and McGovern, D. J. (2016). "Understanding wave generation in pneumatic tsunami simulators." *Proc., 6th Int. Conf., Coastlab16: Application of Physical Modelling in Coastal and Port Engineering and Science*, International Association for Hydro-Environment Engineering and Research.

Chanson, H. (2004). *The hydraulics of open channel flow: An introduction*, 2nd Ed., Elsevier, Oxford, U.K.

Chanson, H. (2005). "Le tsunami du 26 Décembre 2004: un phénomène hydraulique d'ampleur internationale: premiers constats." *La Houille Blanche*, 2, 25–32.

Chanson, H. (2006). "Tsunami surges on dry coastal plains: Application of dam break wave equations." *Coastal Eng. J.*, 48(4), 355–370.

Chanson, H. (2009). "Application of the method of characteristics to the dam break wave problem." *J. Hydraul. Res.*, 47(1), 41–49.

Chanson, H. (2011). "Hydraulic jumps: Turbulence and air bubble entrainment." *La Houille Blanche*, 3, 5–16.

Chanson, H. (2012). "Momentum considerations in hydraulic jumps and bores." *J. Irrig. Drain. Eng.*, 10.1061/(ASCE)IR.1943-4774.0000409, 382–385.

Chanson, H., Aoki, S.-i., and Maruyama, M. (2000). "Experimental investigations of wave runup downstream of nappe impact: Applications to flood wave resulting from dam overtopping and tsunami wave runup." *Coastal/Ocean Engineering Rep. COE00-2*, Dept. of Architecture and Civil Engineering, Toyohashi Univ. of Technology, Toyohashi, Japan.

Chanson, H., Aoki, S.-i., and Maruyama, M. (2002). "Unsteady air bubble entrainment and detrainment at a plunging breaker: Dominant time

scales and similarity of water level variations." *Coastal Eng.*, 46(2), 139–157.
Chanson, H., Aoki, S.-i., and Maruyama, M. (2003). "An experimental study of tsunami runup on dry and wet horizontal coastlines." *Sci. Tsunami Hazards*, 20(5), 278–293.
Chock, G. Y. K. (2015). "The ASCE 7 tsunami loads and effects design standard." *Structures Congress 2015*, N. Ingraffea and M. Libby, eds., ASCE, Reston, VA, 1446–1456.
Chock, G., Robertson, I., Kriebel, D., Francis, M., and Nistor, I. (2013). *Tohoku, Japan, earthquake and tsunami of 2011: Performance of structures under tsunami loads*, ASCE, Reston, VA.
Cross, R. H, III. (1967). "Tsunami surge forces." *J. Wtrwy. Harb. Div.*, 93(4), 201–231.
Dias, P., Dissanayake, R., and Chandratilake, R. (2006). "Lessons learned from tsunami damage in Sri Lanka." *Proc. Inst. Civ. Eng. Civ. Eng.*, 159(2), 74–81.
FEMA. (2001). "Coastal construction manual: Principles and practices of planning, siting, designing, constructing, and maintaining residential buildings in coastal regions." *FEMA 55*, Washington, DC.
Fritz, H. M. (2002). "Initial phase of landslide generated impulse waves." PhD thesis, ETH/VAW Zürich, Zurich, Switzerland.
Fritz, H. M., et al. (2012). "The 2011 Japan tsunami current velocity measurements from survivor videos at Kesennuma Bay using LiDAR." *Geophys. Res. Lett.*, 39(7), 1–6.
Fuchs, H., and Hager, W. H. (2015). "Solitary impulse wave transformation to overland flow." *J. Waterway, Port, Coastal, Ocean Eng.*, 10.1061/(ASCE)WW.1943-5460.0000294, 04015004.
Goseberg, N., Stolle, J., Derschum, C., and Nistor, I. (2017). "Swing gate generated dam-break waves." *Proc., 37th IAHR World Congress, Learning from the Past for the Future*, International Association for Hydro-Environment Engineering and Research.
Goseberg, N., Wurpts, A., and Schlurmann, T. (2013). "Laboratory-scale generation of tsunami and long waves." *Coastal Eng.*, 79, 57–74.
Heller, V. (2007). "Landslide generated impulse waves: Prediction of near field characteristics." Ph.D. thesis, ETH/VAW Zürich, Zurich, Switzerland.
Henderson, F. M. (1966). *Open channel flow*, MacMillan, New York.
Huber, A. (1980). "Schwallwellen in seen als folge von felsstürzen [Impulse waves following rockfalls]." Ph.D. thesis, ETH/VAW Zürich, Zurich, Switzerland.
Iizuka, H., and Matsutomi, H. (2000). "Damage due to flood flow of tsunami." *Proc. Coastal Eng. JSCE*, 47, 381–385.
Jaffe, B. E., Goto, K., Sugawara, D., Richmond, B. M., Fujino, S., and Nishimura, Y. (2012). "Flow speed estimated by inverse modeling of sandy tsunami deposits: Results from the 11 March 2011 tsunami on the coastal plain near the Sendai Airport, Honshu, Japan." *Sediment. Geol.*, 282, 90–109.
Kilburna, C., and Petleyb, D. (2003). "Experimental study of bore-driven swash hydrodynamics on impermeable rough slopes." *Geomorphology*, 54, 21–32.
Kirkoz, M. (1983). "Breaking and run-up of long waves, tsunamis: Their science and engineering." *Proc., 10th IUGG Int. Tsunami Symp.*, Terra Scientific, Tokyo.
Koch, C., and Chanson, H. (2009). "Turbulence measurements in positive surges and bores." *J. Hydraul. Res.*, 47(1), 29–40.
LabVIEW [Computer software]. National Instruments, Austin, TX.
Lauber, G., and Hager, W. H. (1998). "Experiments to dambreak wave: Horizontal channel." *J. Hydraul. Res.*, 36(3), 291–307.
Leng, X., and Chanson, H. (2015). "Breaking bore: Physical observations of roller characteristics." *Mech. Res. Commun.*, 65, 24–29.
Leng, X., and Chanson, H. (2016). "Coupling between free-surface fluctuations, velocity fluctuations and turbulent Reynolds stresses during the upstream propagation of positive surges, bores and compression waves." *Environ. Fluid Mech.*, 16(4), 695–719.
Leng, X., and Chanson, H. (2017a). "Unsteady turbulence, dynamic similarity and scale effects in bores and positive surges." *Eur. J. Mech. B Fluids*, 61, 125–134.
Leng, X., and Chanson, H. (2017b). "Unsteady velocity profiling in bores and positive surges." *Flow Meas. Instrum.*, 54, 136–145.
Liu, P. L.-F., Yeh, H., and Synolakis, C. (2008). *Advances in coastal and ocean engineering: Advanced numerical models for simulating tsunami waves and run-up*, Vol. 10, World Scientific, Singapore.
Madsen, P. A., Fuhrman, D. R., and Schäffer, H. A. (2008). "On the solitary wave paradigm for tsunamis." *J. Geophys. Res. C: Oceans*, 113, 1–22.
Matsutomi, H., and Okamoto, K. (2010). "Inundation flow velocity of tsunami on land." *Isl. Arc*, 19(3), 443–457.
Matsutomi, H., Sakakiyama, T., Nugroho, S., and Matsuyama, M. (2006). "Aspects of inundated flow due to the 2004 Indian Ocean tsunami." *Coastal Eng. J.*, 48(2), 167–195.
Meile, T. (2007). "Influence of macro-roughness of walls on steady and unsteady flow in a channel." Ph.D. thesis, Laboratory of Hydraulic Constructions, École Polytechnique Fédérale de Lausanne, Écublens, Switzerland.
Meile, T., Boillat, J.-L., and Schleiss, A. J. (2011). "Water-surface oscillations in channels with axi-symmetric cavities." *J. Hydraul. Res.*, 49(1), 73–81.
Meile, T., De Cesare, G., Blanckaert, K., and Schleiss, A. J. (2008). "Improvement of acoustic Doppler velocimetry in steady and unsteady turbulent open-channel flows by means of seeding with hydrogen bubbles." *Flow Meas. Instrum.*, 19, 215–221.
Montes, S. (1998). *Hydraulics of open channel flow*, ASCE, Reston, VA.
Murty, T. S. (1977). *Seismic sea waves: Tsunamis*, Dept. of Fisheries and the Environment Fisheries and Marine Service, Ottawa.
Nistor, I., Palermo, D., Nouri, Y., Murty, T., and Saatcioglu, M. (2009). "Chapter 11: Tsunami-induced forces on structures." *Handbook of coastal and ocean engineering*, Y. C. Kim, ed., World Scientific, Singapore, 261–286.
Nouri, Y., Nistor, I., Palermo, D., and Cornett, A. (2010). "Experimental investigation of the tsunami impact on free standing structures." *Coastal Eng. J.*, 52(1), 43–70.
O'Donoghue, T., Pokrajac, D., and Hondebrink, L. J. (2010). "Laboratory and numerical study of dambreak-generated swash on impermeable slopes." *Coastal Eng.*, 57(5), 513–530.
Pfister, M., and Chanson, H. (2012). "Discussions. Scale effects in physical hydraulic engineering models by Valentin Heller, *Journal of Hydraulic Research*, Vol. 49, No. 3 (2011), pp. 293–306." *J. Hydraul. Res.*, 50(2), 244–246.
Ramsden, J. D., (1993). "Tsunami: forces on a vertical wall caused by long waves, bores, and surges on a dry bed." Ph.D. thesis, California Institute of Technology, Pasadena, CA.
Ritter, A. (1892). "Die fortpflanzung der wasserwellen." *Zeitschrift des Verein Deutscher Ingenieure*, 36, 947–954.
Rossetto, T., Allsop, W., Charvet, I., and Robinson, D. (2011). "Physical modelling of tsunami using a new pneumatic wave generator." *Coastal Eng.*, 58(6), 517–527.
Rossetto, T., et al. (2007). "The Indian Ocean tsunami of December 26, 2004: Observations in Sri Lanka and Thailand." *Nat. Hazards*, 42(1), 105–124.
Shafiei, S., Melville, B. W., and Shamseldin, A. Y. (2016). "Experimental investigation of tsunami bore impact force and pressure on a square prism." *Coastal Eng.*, 110, 1–16.
Stoker, J. J. (1958). *Water waves: The mathematical theory with applications*, John Wiley & Sons, New York.
Suppasri, A., Shuto, N., Imamura, F., Koshimura, S., Mas, E., and Yalciner, A. C. (2013). "Lessons learned from the 2011 Great East Japan tsunami: Performance of tsunami countermeasures, coastal buildings, and tsunami evacuation in Japan." *Pure Appl. Geophys.*, 170, 993–1018.
Thusyanthan, N. I., and Madabhushi, S. (2008). "Tsunami wave loading on coastal houses: A model approach." *Proc. Inst. Civ. Eng. Civ. Eng.*, 161(2), 77–86.
Wang, H., and Chanson, H. (2015). "Air entrainment and turbulent fluctuations in hydraulic jumps." *Urban Water J.*, 12(6), 502–518.
Whitham, G. (1955). "The effects of hydraulic resistance in the dam-break problem." *Proc. R. Soc. London, Ser. A*, 227(1170), 399–407.
Wüthrich, D., Pfister, M., De Cesare, G., and Schleiss, A. J., (2016a). "Velocity profile measurements in bore waves." *Proc., 10th Int. Symp., Ultrasonic Doppler Methods for Fluid Mechanics and Fluid Engineering*, Tokyo, 137–140.

Wüthrich, D., Pfister, M., Manso, P., Constantinescu, G., and Schleiss, A. J. (2016b). "Surface turbulence on bores and surges propagating on smooth and rough beds." *Proc., 6th Int. Conf., Coastlab16: Application of Physical Modelling in Coastal and Port Engineering and Science*, International Association for Hydro-Environment Engineering and Research.

Yeh, H. (2007). "Design tsunami forces for onshore structures." *J. Disaster Res.*, 2(6), 531–536.

Yeh, H., Ghazali, A., and Marton, I. (1989). "Experimental study of bore run-up." *J. Fluid Mech.*, 206, 563–578.

Yeh, H. H., and Mok, K.-M. (1990). "On turbulence in bores." *Phys. Fluids A*, 2(5), 821–828.